Received: 11 January 2022 | Revised: 27 September 2022 | Accepted: 14 October 2022

DOI: 10.1111/gbi.12533

gebiology WILEY

ORIGINAL ARTICLE

# Reduction in animal abundance and oxygen availability during and after the end-Triassic mass extinction

Pulkit Singh[1] | Wanyi Lu[2,3] | Zunli Lu[2] | Adam B. Jost[4] | Kimberly Lau[5] | Aviv Bachan[6] | Bas van de Schootbrugge[7] | Jonathan L. Payne[1]

[1]Department of Geological Sciences, Stanford University, Stanford, California, USA

[2]Department of Earth and Environmental Sciences, Syracuse University, Syracuse, New York, USA

[3]Department of Geology and Geophysics, Woods Hole Oceanographic Institution, Woods Hole, Massachusetts, USA

[4]Department of Earth, Atmospheric, and Planetary Sciences, Massachusetts Institute of Technology, Cambridge, Massachusetts, USA

[5]Department of Geosciences and Earth and Environmental Systems Institute, Penn State University, University Park, Pennsylvania, USA

[6]Ericsson, Santa Clara, California, USA

[7]Department of Earth Sciences, Utrecht University, Utrecht, The Netherlands

**Correspondence**
Pulkit Singh, Department of Geological Sciences, Stanford University, Stanford, CA, USA.
Email: ps33@stanford.edu

**Funding information**
National Science Foundation

## Abstract

The end-Triassic biodiversity crisis was one of the most severe mass extinctions in the history of animal life. However, the extent to which the loss of taxonomic diversity was coupled with a reduction in organismal abundance remains to be quantified. Further, the temporal relationship between organismal abundance and local marine redox conditions is lacking in carbonate sections. To address these questions, we measured skeletal grain abundance in shallow-marine limestones by point counting 293 thin sections from four stratigraphic sections across the Triassic/Jurassic boundary in the Lombardy Basin and Apennine Platform of western Tethys. Skeletal abundance decreased abruptly across the Triassic/Jurassic boundary in all stratigraphic sections. The abundance of skeletal organisms remained low throughout the lower-middle Hettangian strata and began to rebound during the late Hettangian and early Sinemurian. A two-way ANOVA indicates that sample age ($p < .01$, $\eta^2 = 0.30$) explains more of the variation in skeletal abundance than the depositional environment or paleobathymetry ($p < .01$, $\eta^2 = 0.15$). Measured I/Ca ratios, a proxy for local shallow-marine redox conditions, show this same pattern with the lowest I/Ca ratios occurring in the early Hettangian. The close correspondence between oceanic water column oxygen levels and skeletal abundance indicates a connection between redox conditions and benthic organismal abundance across the Triassic/Jurassic boundary. These findings indicate that the end-Triassic mass extinction reduced not only the biodiversity but also the carrying capacity for skeletal organisms in early Hettangian ecosystems, adding to evidence that mass extinction of species generally leads to mass rarity among survivors.

**KEYWORDS**
faunal abundance, mass extinction, ocean redox, skeletal abundance, Triassic–Jurassic extinction

## 1 | INTRODUCTION

Predicting the responses of marine ecosystems to extreme environmental change is a task of immense importance for the 21st century, as such predictions are needed to guide effective conservation strategies. The major mass extinctions of the geological past provide our best empirical constraints on such predictions (Blois et al., 2013; Harnik et al., 2012). These biodiversity crises significantly altered the taxonomic composition and ecological structure of marine ecosystems in response to environmental change (Bambach et al., 2002; Droser et al., 2000; Hull & Darroch, 2013; Wagner et al., 2006).

  

Mass extinctions have traditionally been recognized by rapid reductions in taxonomic diversity at regional to global scales (Bambach, 2006; Raup & Sepkoski, 1982). Taxonomic diversity, however, only partially reflects the evolutionary and ecological effects of mass extinctions. Mass extinction events also impact the biogeographic distributions of taxa (Finnegan et al., 2016; Penn et al., 2018), the relative diversities of different ecological guilds (Dineen et al., 2019; Roopnarine & Angielczyk, 2015; Schubert & Bottjer, 1995), body-size distributions within and among species (Atkinson et al., 2019; Payne, 2005), and the abundances of biomineralizing and bioturbating taxa (Cribb & Bottjer, 2020; Knaust, 2010; Twitchett & Barras, 2004). The relative taxonomic and ecological significances of mass extinction events often differ, meaning that extinction and recovery must be understood through the analysis not only of taxonomic diversity but also of other dimensions of biodiversity and ecosystem function (Droser et al., 2000; Greene et al., 2011; Hull et al., 2011; McGhee et al., 2013). Some of the most taxonomically severe extinction events, such as the Late Ordovician extinction, had comparatively little effect on the structure of ecosystems (Brenchley et al., 2001; Christie et al., 2013). In other cases, the global taxonomic losses do not consistently predict the composition of post-extinction ecosystems. For instance, the end-Permian mass extinction preferentially reduced taxonomic diversity within heavily calcified clades such as corals, brachiopods, and echinoderms relative to moderately calcified clades such as bivalves and gastropods (Knoll et al., 1996; Knoll, Bambach, et al., 2007; Sepkoski et al., 1981), but some earliest Triassic shallow-marine communities remained dominated by crinoids and brachiopods rather than by bivalves and gastropods (Brosse et al., 2019; Greene et al., 2011).

Explaining and predicting differences between the responses of diversity and abundance across intervals of rapid environmental change is one of the most important unsolved problems in the study of mass extinction and the conservation of future biodiversity and ecosystem function. Reduction in animal abundance, either overall or differentially across clades and functional groups, can fundamentally alter the state of an ecosystem even in the absence of extinction. For example, marine defaunation by commercial fishing has caused population blooms of species at lower trophic levels, such as prawns and sea urchins, in some parts of the ocean (Diaz & Rosenberg, 2008; McCauley et al., 2015; Scheffer et al., 2005). On land, the biomass of large mammals has increased over the past several centuries even as their taxonomic diversity has declined due to the enormous increases in the population sizes of humans as well as domestic cattle, pigs, and sheep (Barnosky et al., 2012).

Despite the importance of overall biomass to trophic transfer efficiency and nutrient cycling, the responses of overall biomass within ecosystems to past mass extinction events remains poorly quantified. Only a few studies across the end-Silurian (Bowman et al., 2020), end-Permian (Jacobsen et al., 2011; Payne et al., 2006), and end-Cretaceous (Hull et al., 2011; Sibert et al., 2014) extinctions provide empirical constraint on changes in animal abundance across mass extinction intervals. The key pattern emerging from this work is that changes in organismal abundance vary considerably in both time and space across different extinction intervals. These few studies have demonstrated that quantifying animal abundance across mass extinctions in a biogeochemical framework can provide a robust picture of the ecological severity of mass extinctions (Hull, 2015). From a functional standpoint, mass rarity may be as important or more important than the reduction of biodiversity (Hull, 2015).

The end-Triassic mass extinction, ca. 201.5 Ma (Blackburn et al., 2013), was the most taxonomically severe mass extinction experienced by a marine fauna that is taxonomically similar to its modern counterpart (Sepkoski et al., 1981; Ritterbush et al., 2015). The ecological severity of the end-Triassic mass extinction trails only the end-Permian and end-Cretaceous mass extinctions (Bond & Grasby, 2017; McGhee et al., 2013; McGhee Jr et al., 2004). It preferentially impacted the diversity of reef-building taxa like scleractinian corals and sphinctozoan sponges (Dunhill et al., 2018; Hautmann, 2004; Kiessling & Aberhan, 2007; Kiessling et al., 2007). Geological and geochemical data indicate many parallels between the circumstances of the end-Triassic extinction and the "deadly trio" (Pörtner et al., 2004) of climate warming, ocean deoxygenation, and ocean acidification that imperil extant marine animals. During the end-Triassic mass extinction, volcanism in the Central Atlantic Magmatic Province (CAMP) caused the massive injection of isotopically light carbon into the atmosphere (Bachan et al., 2012; Fox et al., 2020; Ruhl & Kürschner, 2011). Sedimentary and geochemical proxy data indicate a resulting drop in the ocean pH (Greene et al., 2011; Jost, Bachan, van de Schootbrugge, Brown, et al., 2017), rise in temperature of about 10°C in the tropics (Pálfy et al., 2007), and expansion of anoxic and euxinic bottom waters (Atkinson & Wignall, 2019; He et al., 2020; Jost, Bachan, van de Schootbrugge, Lau, et al., 2017; Kasprak et al., 2015; Larina et al., 2019; Richoz et al., 2012; Van de Schootbrugge et al., 2007).

Although the taxonomic severity and environmental circumstances of the end-Triassic extinction are increasingly well constrained, their impact on the abundances of animals and other well-fossilized taxa (e.g., foraminifera and calcareous algae) remain essentially unknown due to the lack of relevant data. To fill this knowledge gap, here we quantify changes in organismal abundance across the Triassic/Jurassic transition by generating limestone compositional data across four stratigraphic sections spanning the Triassic/Jurassic boundary in the Tethys realm. By standardizing skeletal content relative to rock volume in carbonate-rich depositional environments and by investigating changes in skeletal content across depositional settings, we provide the first estimate of overall changes in the biomass of skeletal animals, calcareous algae, and foraminifera. Because physiological data and evidence from both the modern ocean (Deutsch et al., 2015) and the end-Permian mass extinction (Penn et al., 2018) indicate that the effects of oxygen availability for aerobic organisms present an important control on extinction and biogeography, we also reconstruct the variation in redox conditions for two of the sections through measurement of I/Ca ratios.

## 2 | GEOLOGICAL SETTING

### 2.1 | Overview

The shallow-marine carbonate sediments exposed in the southern Alps (Lombardy Basin) and southern Apennines of Italy record sedimentation in two distinct paleogeographic domains of western Tethys during the Mesozoic (Figure 1). These paleogeographic domains reflect the Triassic rifting of Pangaea, which led to closure of the Paleo-Tethys Ocean and expansion of the Neotethys Ocean in the Late Triassic (Haas et al., 1995; Schettino & Turco, 2011). As a result of rifting, a series of fault-controlled, intra-platform basins developed across the western Mediterranean. Shallow-marine carbonate platforms developed during this time in the northern and southern parts of western Tethys (Iannace & Zamparelli, 2002; Stampfli et al., 2001). The platforms exposed in the northern, central, and southern Apennines of Italy developed in connection with the Ionian Arm of Tethys, which opened in the Middle Triassic (Ciarapica & Passeri, 2005). Sedimentary deposits of the Northern Calcareous Alps developed in connection with the Alpine Ocean (also referred to as the Ligurian-Piedmont Ocean), which started opening in the Late Triassic to Early Jurassic (Bertotti et al., 1993; Jadoul et al., 2005; Figure 1).

### 2.2 | Lombardy Basin

The Lombardy Basin was in close proximity to the European continent during the Late Triassic and Early Jurassic (Figure 1) and was a site of sediment accumulation in an active rift basin (Berra et al., 2010; Jadoul et al., 1992, 2004). Rifting led to development of horst and graben structures, which became sites of carbonate sedimentation (Jadoul et al., 1992). During the Norian, shallow-marine carbonates accumulated on structural highs and bedded turbiditic limestones accumulated in deeper intra-platform troughs. Rifting slowed during the late Norian and a west-to-east-dipping homoclinal ramp developed (Jadoul et al., 1992, 2004). The Rhaetian-Hettangian ramp carbonates in the Lombardy Basin increase in thickness from west to east due to differential subsidence associated with rifting. Basin-wide marine transgression during the late Hettangian led to deposition of chert-rich sediments of the Sedrina and Moltrasio limestones. The platform ultimately drowned early in the Sinemurian (Jadoul et al., 2004; McRoberts, 1994).

The Rhaetian-Hettangian sedimentary succession in the Lombardy Basin of the south-western Alps consists of shallow-marine ramp carbonates (Galli et al., 2007). The Rhaetian succession of the Lombardy Basin is represented by the Zu Limestone (Figures 2a–c, 3 and 4). The Zu Limestone is a fossiliferous packstone to framestone with a diverse open marine fauna consisting of bivalves, gastropods, and large benthic foraminifera with subordinate corals, brachiopods, ostracods, and echinoderms (Figure 2). The Zu Limestone is abruptly overlain by the Malanotte Formation, which has been assigned a Hettangian age based on pollen content and carbon isotope chemostratigraphy (Van de Schootbrugge et al., 2008). The lower Malanotte Formation is an unfossiliferous marl (Figures 3 and 4). The marl is overlain by carbonate-rich mudstones and wackestones containing rare mollusks (Figure 2). The middle-upper Malanotte Formation is composed of oolitic sands and peloidal packstone indicating a shallowing-upward trend (Galli et al., 2007; Jadoul & Galli, 2008). The Albenza Formation overlies the Malanotte Formation and is composed of oolitic grainstone and oncoidal packstone indicating deposition in a shallow-marine environment (Figures 2–5; Galli et al., 2007; Jadoul & Galli, 2008). The Albenza Formation carbonates also contain some stratigraphically

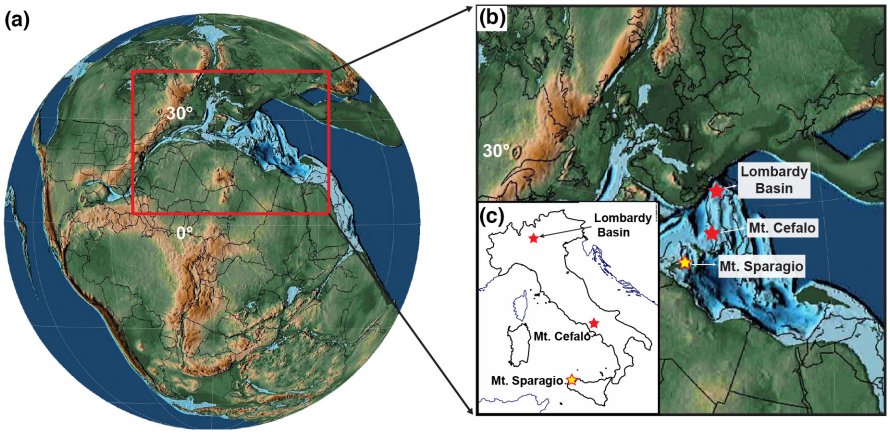


FIGURE 1 Paleogeography and study site locations. Panel (a) shows the Early Jurassic paleogeography modified using the GPLATES software. Panel (b) indicates the paleogeographic locations of the Lombardy Basin (southern Alps), Mt. Cefalo (southern Apennines), and Mt. Sparagio (Sicily) sections in the Tethys Sea. Panel (c) shows the present-day locations of aforementioned sections in Italy. The GPS coordinates for the sections studies in this study are as follows: Italcementi: 45°46′33.83″N 9°31′9.91″E, Val Adrara: 45°43′29.33″N 9°57′32.29″E, Pozzo Glaciale: 45°41′5.99″N 10°2′56.83″E, Mt. Cefalo: 41°15′32.05″N 13°32′10.50″E. The approximate location of Mt. Sparagio section was obtained from He, Newton, et al. (2022). The paleogeographic maps are from Scotese (2016). The outline map of Italy was downloaded from www.d-maps.com using this link: https://d-maps.com/carte.php?num_car=2322&lang=en.

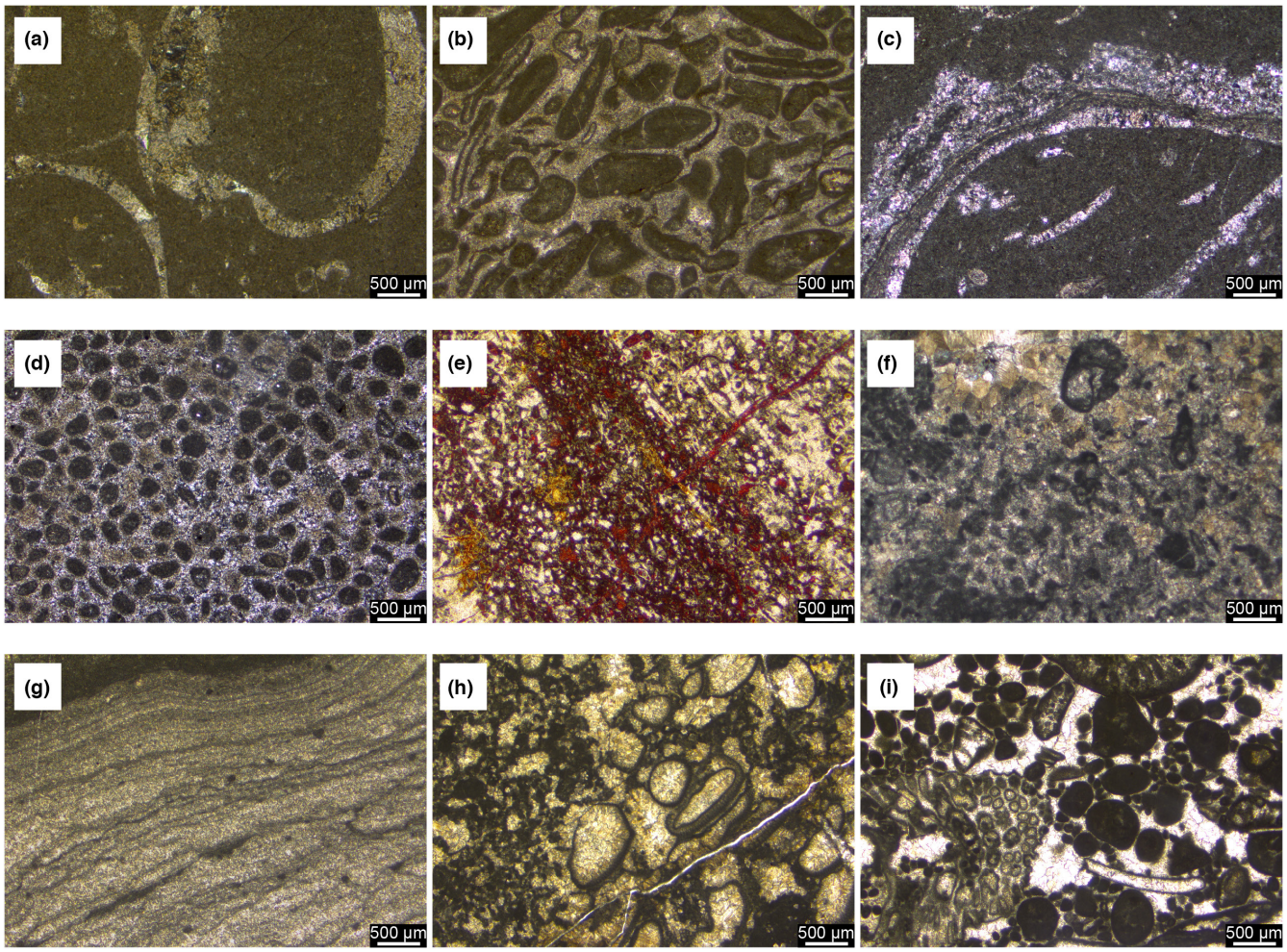


FIGURE 2 Thin section photomicrographs illustrating microfacies from the Lombardy Basin and Apennine Platform. (a) Skeletal packstone from the Rhaetian Zu Limestone showing megalodontid bivalve fragments (Italcementi section), (b) Peloidal grainstone from the Rhaetian Zu Limestone (Italcementi section), (c) Bivalve-rich skeletal packstone from the Rhaetian Zu limestone (Val Adrara section), (d) Oolitic grainstone from lower Hettangian Albenza Formation (Val Adrara section), (e) Sponge spicules from early Sinemurian Moltrasio Limestone (Pozzo Glaciale section), (f)The Rhaetian association of dasyclad green algae (Gryphoporella curvata) and problematic algae (Thaumatoporella parvovesiculifera) from Mt. Cefalo section, (g) Laminar stromatolites from the early Hettangian (Mt. Cefalo section), (h) Problematic algae in a clotted microbial fabric (lower Hettangian, Mt. Cefalo section), (i) Open-marine, subtidal assemblage of calcareous green algae, bivalves, and peloids in upper Sinemurian-lower Pliensbachian Mt. Cefalo section.

limited intervals exhibiting fabric-destructive dolomitization. The Sedrina Limestone, which overlies the Albenza Formation, is a cherty, sponge-rich limestone at the Val Adrara locality. It is composed of thin- to medium-bedded mudstones and wackestones and lacks visible bedforms, thus indicating deposition in a deep-water, distal ramp setting (Bachan et al., 2012; McRoberts, 1994). At the Pozzo Glaciale section, the Sedrina Limestone is composed of oncolitic and oolitic grainstone to packstone, indicating deposition in a subtidal, open-marine environment (Jadoul & Galli, 2008; McRoberts, 1994; Figures 3–5). The Pozzo Glaciale section has been interpreted as the eastern margin of the Lombardian Platform (Figure 5; Jadoul & Galli, 2008; McRoberts, 1994). The Moltrasio Limestone, which overlies the entire Lombardy Basin, is composed of chert-bearing mudstone and marks the final drowning of the Lombardian Platform (Figure 2; Jadoul & Galli, 2008; McRoberts, 1994).

In this study, we analyzed hand samples from the three measured stratigraphic sections within a broad shallow-to-deep depositional gradient in the Lombardy Basin: Italcementi, Val Adrara, and Pozzo Glaciale (Figures 3–5). The sections can be correlated based on the formation boundaries, supplemented by carbon isotope chemostratigraphy (Bachan et al., 2012; Galli et al., 2005). Biostratigraphic age assignments are based on Gaetani (1970), Lakew (1990, 1994), McRoberts (1994), and Muttoni et al. (2010).

## 2.3 | Apennine Platform

The Mt. Cefalo section is part of the vast, shallow-marine carbonate succession of the Apennine Platform (Figure 1). It was deposited in the south-western Tethys close to the deep-water, Ionian arm of

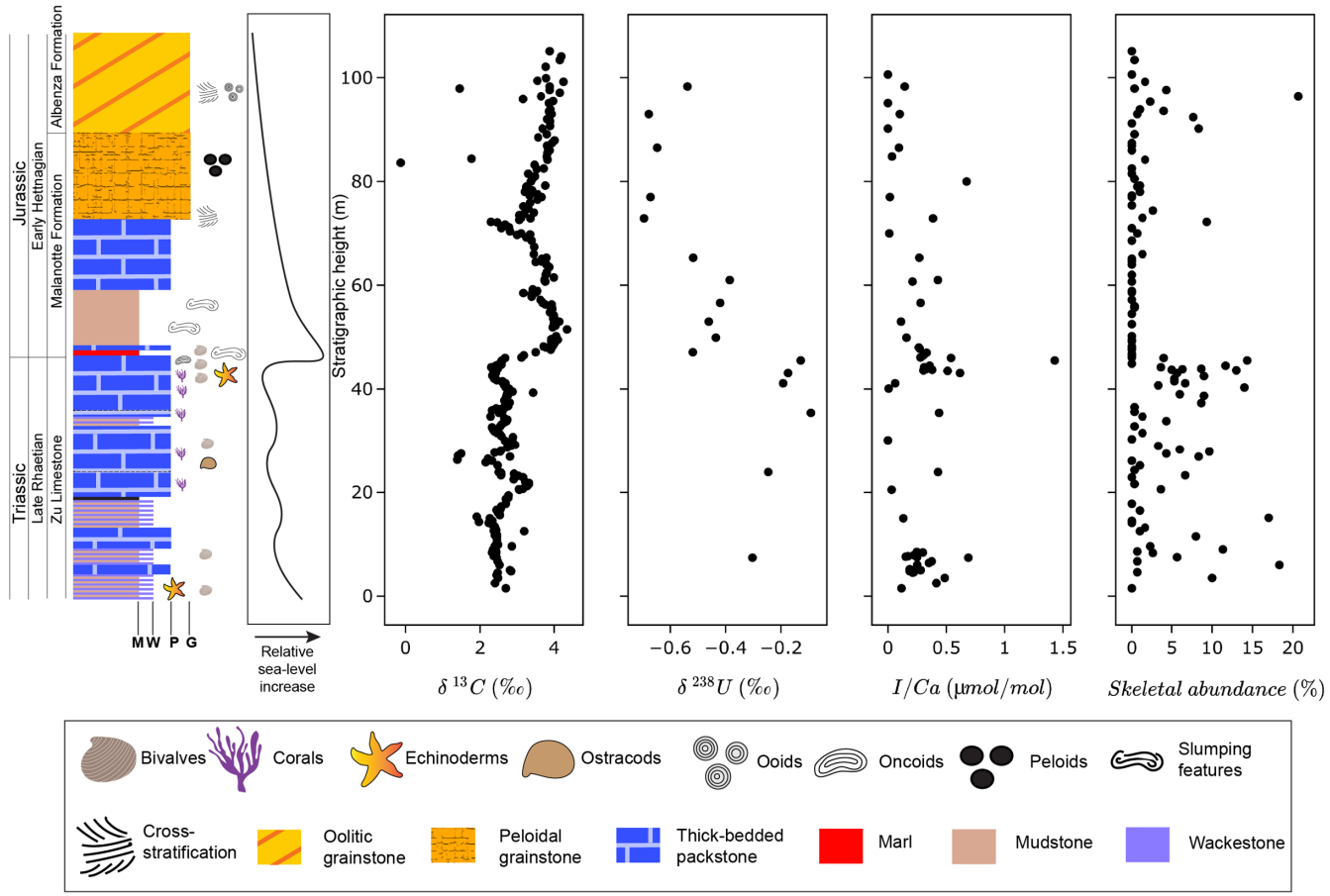


FIGURE 3 The variations in carbonate carbon isotope ratios ($\delta^{13}C$; Bachan et al., 2012), uranium isotopes ratios ($\delta^{238}U$; Jost, Bachan, van de Schootbrugge, Lau, et al., 2017), I/Ca ratios and skeletal abundance at the Italcementi section in the Lombardy Basin (this study).

Tethys. The peritidal sedimentary successions from this shelf are exposed in the central and southern Apennines (Di Stefano et al., 2015; Mancinelli et al., 2005), western Sicily (Todaro et al., 2016, 2017), Greece (Romano et al., 2008), and Turkey (Coskun Tunaboylu et al., 2014).

The measured section is part of a thick Mesozoic carbonate succession deposited from the Late Triassic to Cretaceous in the northern, central, and southern Apennines of Italy (Figure 6). The sediments from Mt. Cefalo were deposited in a shallow-marine, peritidal environment (Bachan et al., 2012; Mancinelli et al., 2005). The meter-scale cycles at Mt. Cefalo, the shallowest section of our four sections, are typically composed of allochem-rich packstone and grainstone capped by fenestral boundstones (Figure 2). The cycles alternate between microfacies containing clotted and filamentous microbialites exhibiting fenestral fabrics indicating an intertidal to supratidal depositional environment and microfacies containing calcareous algae and benthic foraminifera and lacking fenestral fabrics, suggesting deposition in a shallow subtidal to restricted lagoon setting (Bachan et al., 2012; Mancinelli et al., 2005). The Rhaetian fossil assemblage is dominated by dasyclad green algae (*Gryphoporella curvata*), large benthic foraminifera (*Triasina hantkeni*), megalodontid bivalves, gastropods, echinoderms, ostracods, and problematic algae (*Thaumatoporella parvovesiculifera*; Figure 2). The Hettangian-lower Sinemurian (110–270 m) assemblage is distinguished by an absence of megalodontid bivalves, dasyclad algae, and large benthic foraminifera. The Hettangian-lower Sinemurian biota is dominated by problematic algae with minor mollusks. Dasyclad algae reappear and become more common in the upper Sinemurian-lower Pliensbachian strata (270–325 m) along with a rich assemblage of large benthic foraminifera (Mancinelli et al., 2005; Figure 2).

## 3 | MATERIALS AND METHODS

The samples used in this study were collected from four measured stratigraphic sections, three from the Lombardy Basin (Figures 3–5) in the southern Alps and one (Mt. Cefalo) from the Apennine Platform (Figure 6) in the southern Apennines. The hand samples were used for the compositional analysis and I/Ca measurements. A total of 370 (Italcementi: 159, Val Adrara: 169, Pozzo Glaciale: 42) samples were studied from the Lombardy Basin, and 67 samples were studied from the Apennine Platform section at Mt. Cefalo. The number of samples analyzed for both composition and I/Ca

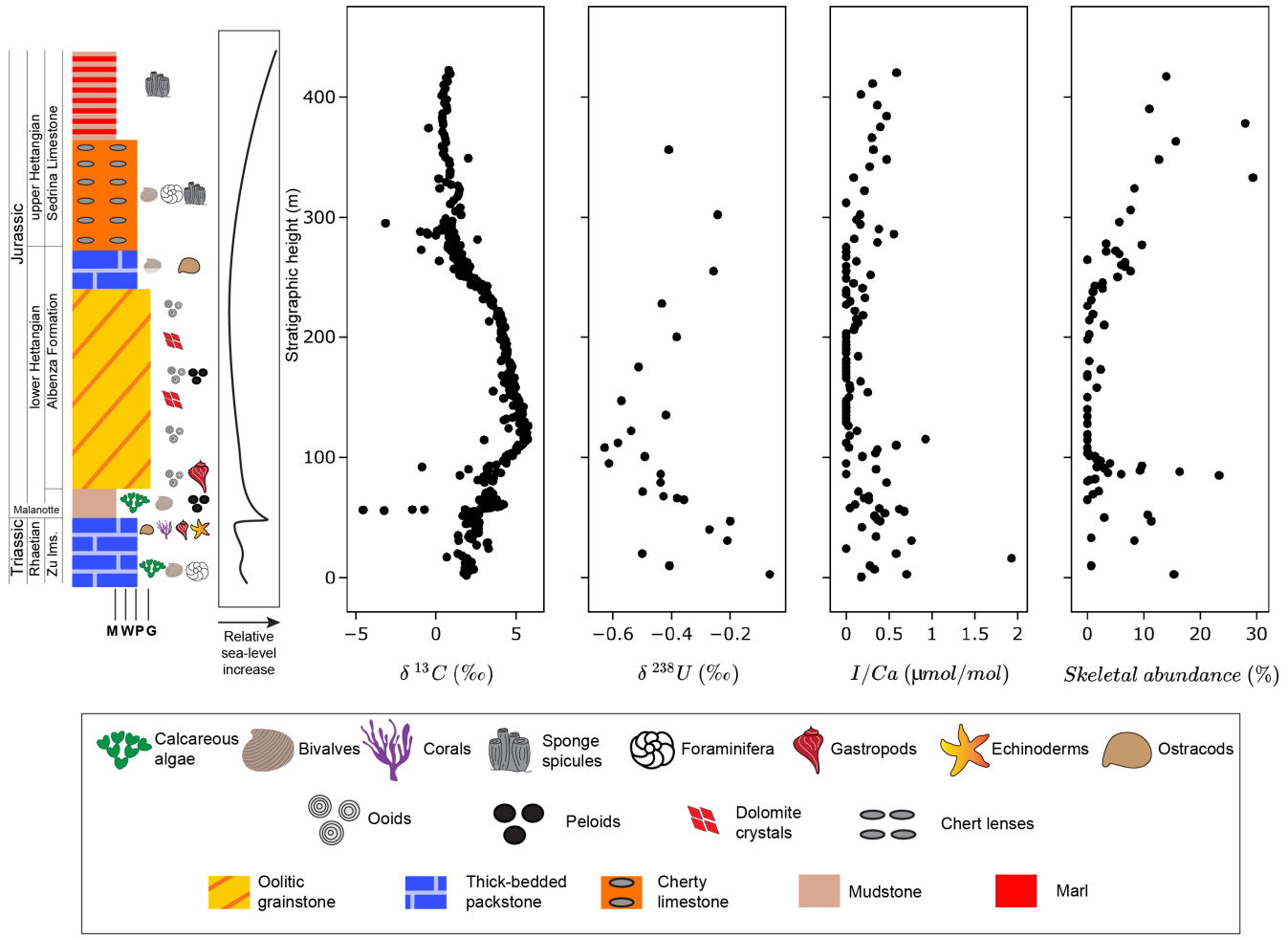


FIGURE 4 The variations in carbonate carbon isotope ratios ($\delta^{13}C$; Bachan et al., 2012; Van de Schootbrugge et al., 2008), uranium isotopes ratios ($\delta^{238}U$; Jost, Bachan, van de Schootbrugge, Lau, et al., 2017), I/Ca ratios and skeletal abundance at the Val Adrara section in the Lombardy Basin (this study). The age model is based on Bachan and Payne (2016).

ratio amounted to 26 and 15 for the Italcementi Val Adrara sections, respectively.

## 3.1 | Compositional analysis of marine limestones

In this study, a total of 293 samples: 112, 72, 42 from Italcementi, Val Adrara, and Pozzo Glaciale, respectively, and 67 from Mt. Cefalo were chosen for thin sectioning. The proportional content of grains, matrix, cement, and void space was quantified via compositional analysis. Compositional analysis was conducted by counting 300 points per thin section (size: 26×46 mm) across the Rhaetian-Hettangian interval in the Lombardy Basin and Mt. Cefalo section from the Apennine Platform (Table S1). Specifically, samples were point-counted using a mechanical stage following the grain-solid method (Flügel, 2010). Skeletal grains were assigned to higher taxonomic groups when identifiable, down to the Linnaean class level where possible. The categories used for compositional analysis were: bivalves, gastropods, brachiopods, echinoderms, ostracods, corals, bryozoans, sponges, foraminifera, red algae, green algae, problematica, unidentified biota, filamentous microbial fabric, clotted microbial fabric, micrite, micrite clasts, peloid, radiaxial fibrous calcite cement, blocky calcite cement, microsparite, dolomite, and ooids. The microbial components were point-counted by the presence of clotted and filamentous fabric in thin sections. Microbial components were not included in the calculation of total skeletal abundance calculation, which focused on enzymatically controlled carbonate skeletons.

The diversity of skeletal components in limestone samples was quantified by a comprehensive survey of each thin section. The diversity of a thin section is represented by the number of distinct taxonomic categories observed (Table S2). The total diversity of a thin section was quantified as the number of distinct categories of enzymatically controlled skeletal grains present in the thin section (see above for the categories used). For instance, if a thin section contained only calcareous algae and bivalves, then its diversity would be noted as two. This approach ensured that a skeletal grain that was not counted while point counting would still be accounted for in the total diversity.

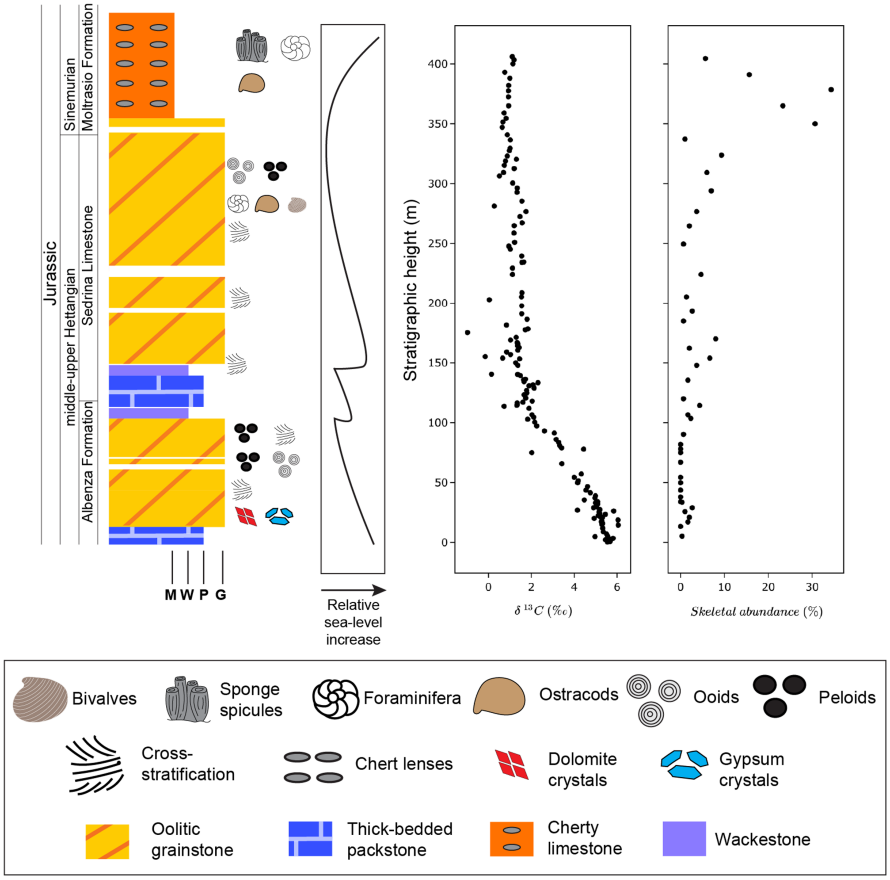


FIGURE 5 The variations in carbonate carbon isotope ratios ($\delta^{13}C$; Bachan et al., 2012; Van de Schootbrugge et al., 2008) and skeletal abundance at the Pozzo Glaciale section in the eastern edge of Lombardy Basin (this study).

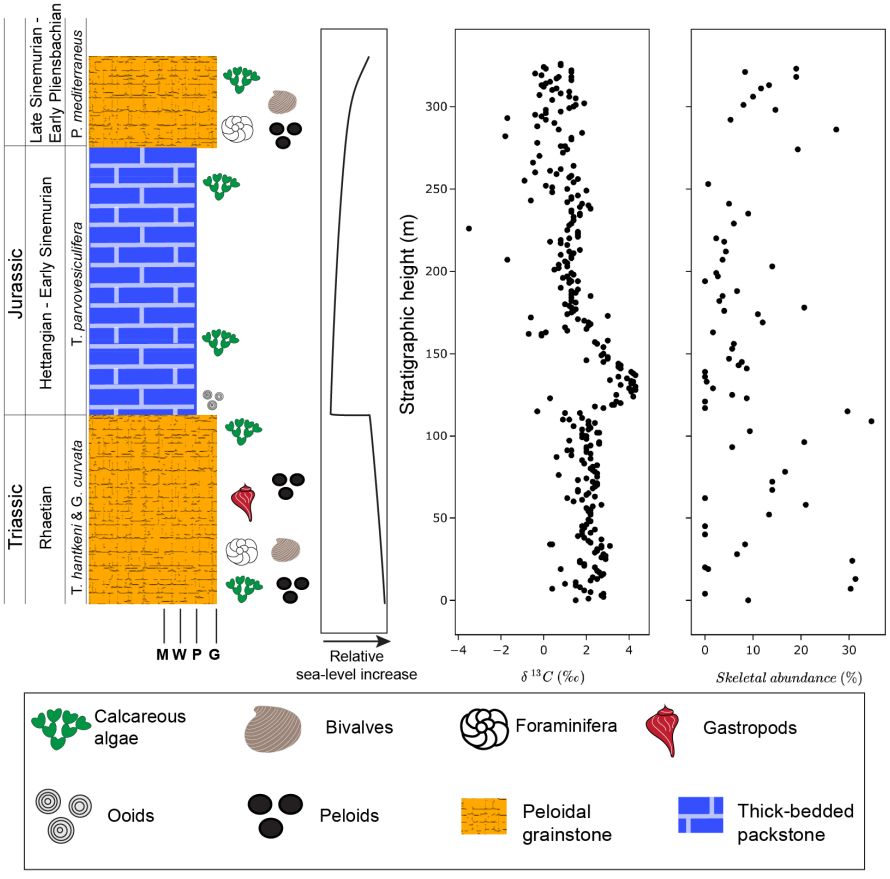


FIGURE 6 The variations in carbonate carbon isotope ratios ($\delta^{13}C$; Bachan et al., 2012) and skeletal abundance in the Mt. Cefalo section of the Apennine platform (this study).

### 3.2 | I/Ca as a redox proxy

The I/Ca ratio of marine limestone has been established as a paleo-proxy for shallow-marine redox conditions (Hardisty et al., 2017; Lu et al., 2010, 2018; Zhou et al., 2014, 2015). The residence time of iodine in seawater is ~300 ky, which is much greater than the seawater circulation time (~1 ky). Although the concentration of iodine in the ocean can be assumed to be globally uniform (Chance et al., 2014), its speciation is spatially variable. The dissolved inorganic iodine is dominantly present in its thermodynamically stable forms of iodate ($IO_3^-$) and iodide ($I^-$) ions in seawater (Wong & Brewer, 1977). The standard reduction potential of $IO_3^-/I^-$ is very close to that of $O_2/H_2O$, thus making the speciation of iodine very sensitive to dissolved oxygen concentrations. In oxic conditions, most iodine occurs as iodate and is reduced to iodide in dysoxic to anoxic conditions.

In the modern ocean, the concentration of iodate qualitatively tracks the concentration of dissolved oxygen in seawater (Lu et al., 2016; Truesdale et al., 2000). In the well-oxygenated upper ocean, iodate is the dominant iodine species whereas in anoxic basins and in oxygen minimum zones (OMZs), iodide is dominant (Emerson et al., 1979; Wong & Brewer, 1977). During formation of carbonate sediment, only iodate is incorporated into the carbonate lattice (Lu et al., 2010). Consequently, the concentration of iodine relative to calcium in limestone is sensitive to the dissolved oxygen concentration in the seawater from which it was precipitated (Lu et al., 2010).

In total, 104 samples from the Val Adrara and Italcementi sections of the Lombardy Basin were analyzed for I/Ca ratios following the methods of Lu et al. (2018; Table S3). The I and Ca concentrations were measured on a Bruker M90 quadrupole inductively coupled plasma mass spectrometer (ICP-MS) housed at Syracuse University. For the analysis, 3–5 mg of powdered limestone (extracted using 0.8 mm drill bit) samples were weighed out, thoroughly rinsed with de-ionized water, and then dissolved in 3% $HNO_3$ acid. The solutions were diluted for analysis to achieve ~50 ppm Ca. To stabilize iodine, 0.5% tertiary amine solution was added to each solution. For analysis, 5 ppb of Sc and Cs were added as internal standards. The detection limit of I/Ca is around 0.1 μmol/mol. The sensitivity of $^{127}I$ is tuned to about 80–100 kcps for a 1 ppb standard. The precision of $^{127}I$ is typically better than 1%. The long-term precision is assessed with repeated measurements of the reference material JCp-1 (Lu et al., 2010) and was 3.70 ± 0.27 μmol/mol (1$\sigma$) ($n$ = 2280; Lu et al., 2020). The I/Ca values of samples were corrected by adjusting the value of the adjacent JCp-1 measurements to 4.

## 4 | RESULTS

### 4.1 | Compositional analysis of marine limestones

The Lombardy Basin and the Apennine Platform both record a drop in skeletal abundance across the Triassic–Jurassic boundary (Figures 3–6). All three stratigraphic sections indicate a statistically significant change in the skeletal abundance across the Upper Triassic and Lower Jurassic time intervals (binned into time intervals defined by the stratigraphic or biostratigraphic constraints for each stratigraphic section as depicted in Figures 3–6; one-way ANOVA results: Mt. Cefalo: $p < .01$, Italcementi: $p < .01$, Val Adrara: $p = .01$; Figure 7). Furthermore, a two-way ANOVA on all 293 samples across the four stratigraphic sections shows that the time interval ($p < .01$, $\eta^2 = 0.30$) explains more of the variation in skeletal content than which stratigraphic section the sample is from ($p < .01$, $\eta^2 = 0.15$). To test this finding further, we conducted another two-way ANOVA consisting of samples from the same ramp, but different water depths from the Italcementi and Val Adrara sections. The results again showed similar results with more of the variation in skeletal abundance explained by time interval ($p < .01$, $\eta^2 = 0.37$) than by stratigraphic section ($p < .01$, $\eta^2 = 0.12$).

The composition of skeletal material across Lombardy Basin and Apennine Platform stratigraphic sections differed significantly depending on the depositional environment and time interval (Figure 7). The main difference between the Lombardy Basin and Apennine Platform limestones is the dominance of non-poriferan animals as skeleton producers in the Lombardy Basin whereas calcareous algae and protists are the skeletal grains in the Apennine Platform (Figure 7). The Rhaetian Zu Limestone at Italcementi and Val Adrara is primarily composed of non-poriferan animal skeletons (~80%) with protists and calcareous algae forming a minor (<5%) component of skeletal material. The proportion of non-poriferan animal skeletal material as a fraction of all skeletal material decreased in the lower Hettangian strata in both Italcementi and Val Adrara sections whereas the proportion of calcareous algae increased. In the upper Hettangian Sedrina limestone, the Val Adrara locality shows evidence of a rapid increase of water depth evident from the well-bedded carbonate mudstone-wackestone facies rich in sponge spicules floating in a micritic matrix (Bachan et al., 2012; McRoberts, 1994). The skeletal component of limestones at this location is primarily hexactinellid sponges (88%) with minor contributions from non-poriferan calcifying animals and protists. This composition contrasts with that of Pozzo Glaciale, where the identifiable skeletal components are entirely composed of non-poriferan animals and protists. The deepening trend continued across the entire Lombardy Basin during the late Sinemurian and led to deposition of the Moltrasio Limestone, which primarily contains hexactinellid sponges (89%; Figures 4, 5, 7).

In the Apennine Platform, the peritidal facies at Mt. Cefalo are primarily composed of calcareous algae (>75%) in the Rhaetian and Hettangian-early Sinemurian strata (Figure 7). The composition of skeletal material changed significantly in the upper Sinemurian and lower Pliensbachian strata with a significant contribution from benthic foraminifera (~40%) and animals (~22%).

Similar to the skeletal abundance trends, the mean (and median) diversity per sample dropped significantly across the Triassic–Jurassic boundary in both Lombardy Basin and Apennine Platform sections (one-way ANOVA analysis, Mt. Cefalo: $p < .01$, Italcementi: $p < .01$, Val Adrara: $p < .01$; Figure 7). The variations in taxonomic diversity across the four stratigraphic sections are more strongly

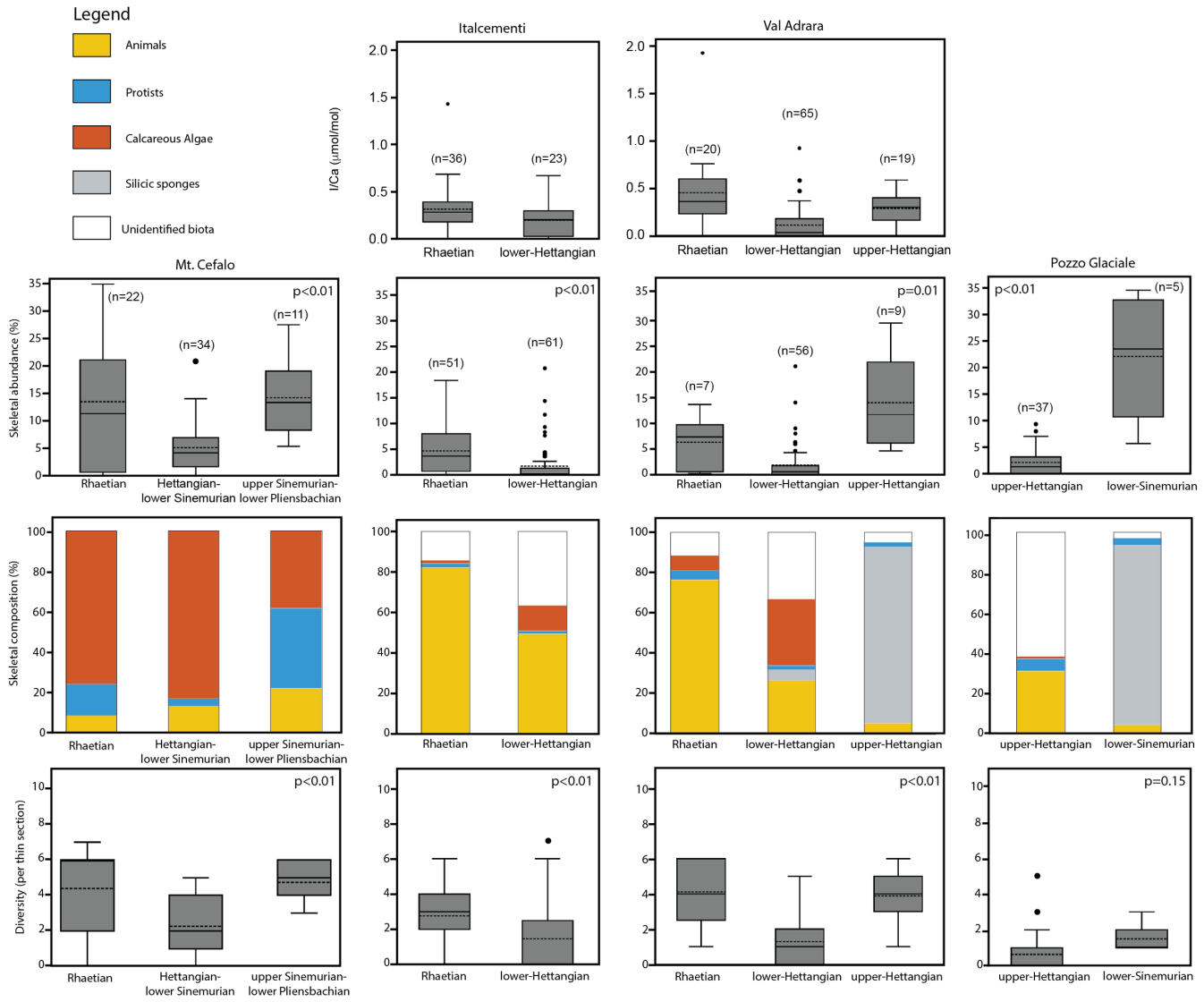


**FIGURE 7** Box plots showing changes in I/Ca ratios, skeletal abundance, skeletal composition, diversity (per thin section) in Upper Triassic and Lower Jurassic limestones from the Lombardy Basin (Italcementi, Val Adrara, Pozzo Glaciale) and Apennine Platform (Mt. Cefalo) sections. "*n*" indicates the number of samples in each category. The figure broadly depicts significant changes in the skeletal abundance, biotic composition, and diversity in marine ecosystems during the Triassic/Jurassic transition along with the redox chemistry as depicted by I/Ca ratios.

associated with changes in time interval (two-way ANOVA: $p < .01$, $\eta^2 = 0.19$) than with the identity of the stratigraphic section (two-way ANOVA: $p < .01$, $\eta^2 = 0.09$). Furthermore, the frequency with which biota from dominant taxonomic categories occurred in samples also decreased sharply across the Triassic–Jurassic boundary (Figure S1).

## 4.2 | I/Ca ratios of bulk carbonate samples

Iodine/calcium background values in both sections are generally low (<2 µmol/mol). The I/Ca ratios decline between the Rhaetian and Hettangian at both Italcementi and Val Adrara (Figures 3, 4, 7). These declines are statistically significant or marginally significant in both the Val Adrara (one-way ANOVA: $p < .01$) and Italcementi (one-way ANOVA: $p = .05$) sections (Figure 7). The limestone samples from the Rhaetian (Zu Limestone) of the Lombardy Basin show I/Ca ratios in the range of <0.01–0.70 µmol/mol (Figures 3 and 4). In the Italcementi section, the mean I/Ca ratio is 0.30 ± 0.25 µmol/mol ($1\sigma$, $n = 36$) whereas the Val Adrara section shows a slightly higher mean I/Ca ratio of 0.45 ± 0.40 µmol/mol ($1\sigma$, $n = 20$; Figures 2 and 3). Overall, the I/Ca ratios in the Rhaetian Zu Limestone of Lombardy Basin decrease towards the Rhaetian-Hettangian boundary. The decreasing trend continues into the lower Hettangian Malanotte and Albenza formations. At the Italcementi section, the mean I/Ca ratio is 0.20 ± 0.16 µmol/mol ($1\sigma$, $n = 23$) whereas in the Val Adrara section, the mean I/Ca ratio is 0.10 ± 0.17 µmol/mol ($1\sigma$, $n = 65$) in the lower-Hettangian strata. In the upper Hettangian Sedrina limestone

exposed only at Val Adrara locality, the I/Ca ratio shows a slight increasing trend towards the top of the section and reaches a mean ratio of 0.28 ± 0.16 μmol/mol (1$\sigma$, $n$ = 19; Figures 3 and 4).

## 5 | DISCUSSION

### 5.1 | Ecological changes across the Triassic/Jurassic boundary in the Lombardy Basin

The compositional changes in shallow-marine carbonates across the Triassic–Jurassic boundary in the Lombardy Basin and Apennine Platform indicate a significant decrease in the abundance and diversity of marine organisms in shallow-marine ecosystems across the extinction interval that cannot be explained by local facies variation (Figure 8). The decrease in skeletal abundance and diversity occurs across a variety of depositional environments ranging from proximal to distal ramp environments of the Lombardy Basin and to peritidal environments of the Apennine Platform. In addition, variation in skeletal content among time intervals is larger than variation among stratigraphic sections. Thus, the observed variations in the skeletal abundance are best interpreted to reflect an external control acting across all sampled locations irrespective of the depositional setting.

The decrease in skeletal content across the Triassic/Jurassic boundary cannot be explained by related changes in the depositional environments represented across the two basins (Figure 8). In the Lombardy Basin, the Rhaetian Zu Limestone is dominantly composed of open-marine fauna deposited in a shallow-marine environment in both the proximal ramp section at Italcementi and the more distal section at Val Adrara. The overlying Malanotte Formation is composed of marls overlain by thin-bedded carbonate mudstones indicating a rise in relative sea level (Bachan et al., 2012). This abrupt change in carbonate sedimentation has been interpreted as a transgressive event that can be traced across the Lombardy Basin and into the Northern Calcareous Alps of western Tethys (McRoberts et al., 1997). The subsequent shallowing indicated by deposition of cross-bedded oolitic and peloidal limestones of the Albenza Formation did not, however, coincide with an increase in skeletal grain abundance. Instead, the skeletal abundance decreased sharply in the lower-middle Hettangian Malanotte Formation and stayed low throughout the lower-middle Hettangian Albenza Formation. The low skeletal abundance at both Italcementi (proximal ramp) and

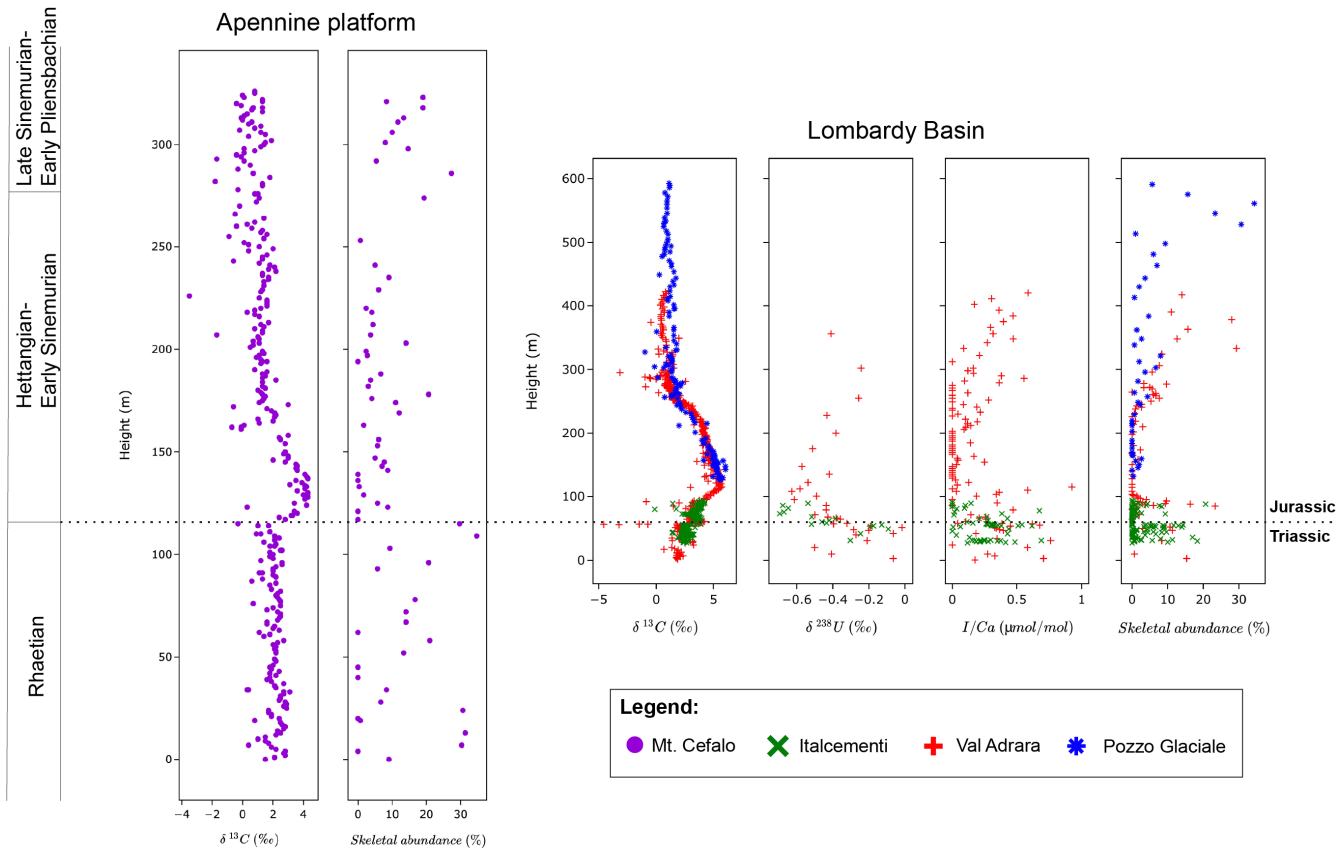


FIGURE 8 A composite plot of variations in stable isotope proxies, I/Ca ratios and skeletal abundance in Lombardy basin and Apennine platform. See Figures 3–6 for data sources. The figure indicates broad-scale spatial and temporal changes in the abundance of skeleton-forming organisms across the Triassic/Jurassic boundary in context of local (I/Ca) and global ($\delta^{238}$U) redox proxies and carbon isotope ratios. The local and global redox proxies indicate a shift to reducing redox conditions in the Lower Jurassic. The negative and positive carbon isotope excursions in Lower Jurassic are global in extent and can be tracked across multiple basins. See Bachan et al. (2012) for detailed description of carbon cycle changes across the Triassic/Jurassic boundary.

Val Adrara (distal ramp) sections indicates that this pattern is not an artifact of local high-energy environments but was a common occurrence across the entire ramp of Lombardy Basin during that time.

This pattern of reduced skeletal abundance and a shift to a non-skeletal carbonate factory also occurs at the Mt. Cefalo section and across the entire Apennine Platform (Barattolo & Romano, 2005; Brandano et al., 2016; Mancinelli et al., 2005; Todaro et al., 2017). The skeletal content at Mt. Cefalo is consistent with observations of physical sedimentary structures that indicate deposition in a peritidal environment across the Rhaetian/Hettangian transition (see Bachan et al. (2012) for detailed stratigraphy). The Rhaetian intertidal facies are composed of stromatolitic laminites whereas the subtidal facies are composed of bioturbated limestones rich in large benthic foraminifera (*T. hantkeni*) and calcareous algae (*G. curvata*). The Triassic/Jurassic boundary is marked by a subaerial exposure surface associated with a sea-level drop that can be traced across the entire Apennine Platform (Berra, 2012; Cirilli et al., 2015; Todaro et al., 2017). The limestone immediately above the exposure surface is oolitic grainstone containing very little skeletal material, indicating the demise of the biological carbonate factory and a shift to a non-skeletal mode of carbonate precipitation. The oolitic limestones are overlain by laminated fenestral boundstones indicating a microbial mode of carbonate precipitation with few intervals rich in calcareous algae but almost devoid of animals and protists. The compositional data from Mt. Cefalo indicate that ecosystems in peritidal environments contained few skeletal animals following the end-Triassic mass extinction and that carbonate precipitation was dominantly abiotic and microbially induced. This shift from metazoan-dominated to microbial and abiotic modes of carbonate precipitation in early-Hettangian is not unique to Mt. Cefalo: compositional data from northern and central Apennines (Brandano et al., 2016) show similar shifts in limestone composition across the Triassic/Jurassic boundary. This finding further supports the interpretation that the facies shifts at Mt. Cefalo are indicative of a more widespread pattern in carbonate deposition rather than a local shift in the depositional environment. The facies pattern in upper Hettangian-lower Sinemurian at Mt. Cefalo records a shift in sedimentation in an open marine peritidal environment with thicker subtidal intervals. However, the overall metazoan abundance remained low throughout the Hettangian and early Sinemurian indicating that the changes in biotic abundance transcended the shift in depositional environment (Figure 6).

Like the abundance patterns, the diversity data is also indicative of a biotic crisis at the end of the Triassic period in Lombardy Basin and Apennine platform. The overall diversity of taxa per sample decreased sharply across the Triassic–Jurassic transition. The fossil occurrences of dominant taxonomic categories when plotted as the percentage of samples in which they appear indicate not only that the taxa became less abundant but also that the frequency with which they occurred decreased substantially (Figure S1).

The close similarities in skeletal abundance and diversity patterns across the Triassic/Jurassic boundary between the widely separated regions (~500 km) of the Lombardy Basin and the Apennine Platform are also representative of a more general pattern across the western Tethys. This pattern of reduced animal abundance across the Triassic/Jurassic boundary followed by establishment of abiotic and microbial carbonate factories during the Early Jurassic occurred also in the Northern Calcareous Alps in Austria (McRoberts et al., 1997), the Transdanubian Range in Hungary (Pálfy et al., 2021), the central and northern Apennines of Italy (Barattolo & Romano, 2005; Brandano et al., 2016; Mancinelli et al., 2005), western Sicily (Todaro et al., 2017, 2018), Greece (Romano et al., 2008), and Turkey (Coskun Tunaboylu et al., 2014). The recovery of skeletal abundance to pre-extinction levels in shallow-marine environments across western Tethyan carbonate platforms occurred in upper Hettangian-Sinemurian limestones with an increase in skeletal contribution from protists and mollusks. Overall, the Early Jurassic ecosystems of western Tethys supported far less benthic biomass and diversity than their Late Triassic counterparts.

The changes in shallow-marine ecosystems in the western Tethys are also representative of a global biotic crisis that unfolded at the end of the Triassic. In the southern Tethys, the shallow-marine platforms of the Arabian plate record a decrease in skeletal abundance across the Triassic/Jurassic boundary and a shift to an abiotic carbonate factory dominated by ooids (Al-Suwaidi et al., 2016; Ge et al., 2018). Evidence from eastern Panthalassa indicates a different extinction pattern than Tethyan sections. During the Early Jurassic, calcifying organisms decreased in abundance and were replaced by silicic demosponges in middle- to inner-ramp environments in Peru (Corsetti et al., 2015; Ritterbush et al., 2014, 2015) and Nevada (Ritterbush et al., 2015, 2016). The post-extinction facies in the Lombardy Basin (this study) and the Eiberg Basin of western Tethys (Delecat & Reitner, 2005) show a similar increase in silicifying hexactinellid sponges in upper Hettangian and lower Sinemurian strata. However, it is challenging to compare them with the Panthalassic ramp sections because the intra-platform basins in the Northern Calcareous Alps experienced a rise in relative sea level beginning in middle-late Hettangian that coincided with an increase in the sponge abundance. Hence, it is unclear whether the increase in abundance of sponges in the Lombardy and Eiberg Basins was a response to the end-Triassic biotic crisis or a response to expansion of deeper marine benthic habitats associated with the rise in relative sea level.

The decrease in the abundance of shell-forming organisms suggests that overall ecological activity decreased sharply across the Triassic/Jurassic transition. The evidence provided above focuses mainly on the composition of carbonate sediments deposited in shallow-marine environments. In theory, the ecological and evolutionary dynamics of shell-forming organisms in carbonate environments could differ from those of skeletal organisms in different environments or from those of non-skeletal organisms. However, evidence of decreased metazoan activity across the Triassic/Jurassic transition is also evident in ichnofacies patterns from both siliciclastic and carbonate environments. The number of ichnotaxa, depth of bioturbation, and size of burrows decreased sharply during late Rhaetian-early Hettangian time in Panthalassic (New York Canyon), Tethyan (Austria) and adjacent ocean basins (southern England; Barras & Twitchett, 2007; Twitchett & Barras, 2004). A sharp decrease in the bioturbation-associated porosity in limestones also occurred in peritidal carbonates of western Tethys (Todaro et al., 2016).

The presence of wrinkle structures in shallow-marine sediments has been associated with reduced metazoan activity in post-extinction environments (Mariotti et al., 2014; Mata & Bottjer, 2009; Pruss et al., 2004). Similar wrinkle structures occur in siliciclastic subtidal environments during the Hettangian (Häntzschel & Reineck, 1968; Peterffy et al., 2016).

The reduction in ecological functioning due to biogeochemical disturbance has occurred multiple times during the Phanerozoic (Aberhan & Kiessling, 2015; Droser et al., 2002; Hull, 2015). The mean total skeletal abundance in comparable peritidal environments was reduced by more than 90% across Permian-Triassic strata (from six stratigraphic sections in South China; Payne et al., 2006) as compared to a ~60% decrease across the Triassic/Jurassic strata (Figure 9). Of the total skeletal abundance, the calcareous algae show an especially interesting response to the end-Permian and end-Triassic extinction events (Figure 8). Macroscopic green algae were ecologically important primary producers during the Paleozoic and early Mesozoic (Hull, 2017; Knoll, Bambach, et al., 2007; Knoll, Summons, et al., 2007; Payne & Van de Schootbrugge, 2007; Wray, 1977). Lower Triassic strata from shallow-marine environments were nearly devoid of calcareous algae in the aftermath of the end-Permian extinction (Bucur, 1999; Payne et al., 2006). Conversely, the calcareous algal abundance in the Lower Jurassic strata decreased only slightly across the Triassic/Jurassic transition (Figure 9). This difference in algal abundance in the aftermaths of the two mass extinctions could indicate that the end-Permian mass extinction was much more severe for calcifying primary producers than the end-Triassic extinction (Bucur, 1999).

## 5.2 | Marine redox conditions and environmental dynamics across the T/J boundary

The I/Ca ratios from the Lombardy Basin most likely record Triassic/Jurassic variations in marine redox conditions. Typical carbonate diagenesis processes, such as alteration by meteoric fluids and dolomitization, can decrease the concentrations of iodate in the carbonate crystal lattice (Hardisty et al., 2017). The elemental ratios of Mg/Ca and Mn/Sr indicate low likelihood of substantial diagenetic alteration in our samples. In the Lombardy Basin samples, there is weak correlation of I/Ca with $\delta^{18}O$ (Pearson corr. [$r$], Italcementi: $r = .27$, $p = .04$, $n = 54$; Val Adrara: $r = .28$, $p = .01$, $n = 81$), of I/Ca with Mg/Ca (Pearson corr. [$r$], Italcementi: $r = .33$, $p = .01$, $n = 54$; Val Adrara: $r = -.03$, $p = .75$, $n = 81$) and of I/Ca with Mn/Sr (Pearson corr. [$r$], Italcementi: $r = .11$, $p = .69$, $n = 13$; Val Adrara: $r = .12$, $p = .43$, $n = 42$; Figure S2). The Mn/Sr ratio, in particular, is indicative of the degree of alteration through meteoric diagenesis (Brand & Veizer, 1980). In theory, the Mn/Sr and I/Ca ratios should be inversely correlated in case of significant diagenesis in the meteoric zone (Hardisty et al., 2017). However, the samples from the Lombardy Basin do not indicate significant inverse correlation between the two ratios. Furthermore, He, Newton, et al. (2022) reported a sharp drop in carbonate I/(Ca+Mg) ratios from a mean of 3.5 µmol/mol during pre-extinction period to 1.4 µmol/mol across the extinction horizon in another Italian section (Mt. Sparagio, Figure 1), independently supporting the temporal trend in local redox conditions observed in this study.

The lithology of the limestones also does not appear to play a major role in governing I/Ca ratios. A one-way ANOVA ($p < .05$,

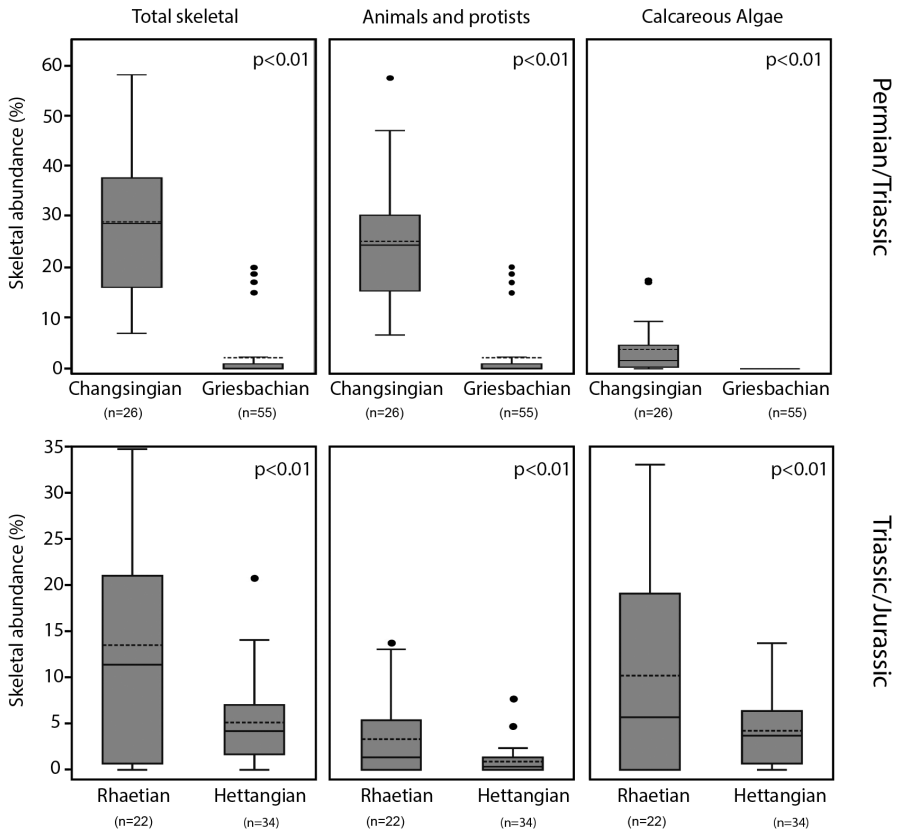


FIGURE 9 Box plots showing skeletal abundance variations in shallow marine environments across two major mass extinction boundaries: end-Permian mass extinction and end-Triassic mass extinction. In the top panel: the leftmost plot shows total skeletal abundance change across Changsingian (Upper Permian) – Griesbachian (Lower Triassic) boundary. The plots in the center and right show a breakdown of total skeletal abundance in animals and protists, and calcareous algae, respectively. The lower panel from left to right: total skeletal, animal and protists, and calcareous algae abundance variations across the Rhaetian (Upper Triassic) – Hettangian (Lower Jurassic) boundary. The data for the end-Permian mass extinction was obtained from Payne et al. (2006). "*n*" indicates the number of thin sections in each category.

$\eta^2 = 0.16$) on the I/Ca ratios of different lithologies encountered in our data indicates that although there are statistically significant differences in the means of different lithologies, this factor overall explains only a minor percentage of variance in the I/Ca ratios (Figure S3). A two-way ANOVA of the Val Adrara section data, with age and lithology as the independent variables, indicates that time period ($p = .04$, $\eta^2 = 0.07$) is a significant predictor of I/Ca ratios whereas the lithology is not ($p = .62$, $\eta^2 = 0.02$). In the Italcementi section, the lithology ($p = .07$, $\eta^2 = 0.45$) similarly explains more of the variation in I/Ca than does the time period ($p = .45$, $\eta^2 = 0.01$) but overall neither time period nor lithology is significantly associated with I/Ca ratios in the two-way ANOVA. The small effect size and lack of statistically significant associations could indicate that I/Ca ratios at Italcementi section have a higher noise/signal ratio than at Val Adrara. The source of noise could be diagenetic and/or lithologic factors. However, the weight of the evidence points to temporal changes in primary I/Ca ratios across the Triassic/Jurassic boundary.

The I/Ca values found in this study are relatively low (<2 μmol/mol), whereas the Rhaetian peritidal limestones from the southwestern Tethys (He, Newton, et al., 2022) have higher I/Ca values. These observations can be explained in two ways: (1) the low I/Ca values in the Lombardy Basin are largely primary signals indicating a low-oxygen water mass in close proximity to the sample locations; or (2) post-depositional diagenetic alteration lowered the primary I/Ca of the rocks after deposition. Support for a low-oxygen water mass (and a primary signal) comes from the argument that the organic matter remineralization depth in the oceanic water column deepened during the Mesozoic, which reduced the prevalence of shallow oxygen minimum zones compared to the Paleozoic (Lu et al., 2018). Although the exact timing of this transition is still unclear, a shallower OMZ in the Triassic is consistent with current evidence, including previously published I/Ca data from the Rhaetian (Lu et al., 2018). For instance, our mean I/Ca values during the Rhaetian (0.30 and 0.45 μmol/mol for Italcementi and Val Adrara respectively) are close to values (0.22 μmol/mol) from the adjacent Lagonegro Basin (Lu et al., 2018). On the other hand, the Rhaetian peritidal limestones from the southwestern Tethys exhibit high I/Ca ratios, around 3.5 μmol/mol (He, Newton, et al., 2022). Therefore, it is possible that some low oxygen waters were close to the Lombardy Basin sections throughout the study interval. Diagenetic loss of carbonate-associated iodine during later diagenesis cannot be completely ruled out, but there is no evidence to suggest that the stratigraphic trend in I/Ca is dominated by diagenesis based on relationships with $\delta^{18}O$, Mg/Ca, and Mn/Sr (Figure S2).

The I/Ca data (0.00–0.70 μmol/mol) from the Upper Triassic of the Lombardy Basin suggest a water column where oxygen was present and relatively stable but not abundant (Figure 8). The subsurface marine redox conditions at the end of the Triassic shifted toward anoxic/hypoxic conditions based on a decrease in I/Ca (Figure 8). Variation in I/Ca ratios indicating an expansion of local dysoxic and anoxic waters across the Triassic/Jurassic boundary is consistent with other lines of evidence for globally widespread anoxic and euxinic water column conditions in shallow marine environments during the Early Jurassic (He, Newton, et al., 2022; He, Wignall et al., 2022). The uranium isotope ratios ($\delta^{238}U$) from the Lombardy Basin record a negative excursion of 0.7‰, indicating a 30-fold increase in anoxic seafloor area in a span of ~45 kyr at the Triassic/Jurassic boundary (Jost, Bachan, van de Schootbrugge, Lau, et al.,2017). Anoxia-driven isotopic excursions have also been interpreted from carbonate-associated sulfate ($\delta^{34}S$) isotope ratios (He et al., 2020). The evidence of photic zone euxinia in shallow-marine environments across the Triassic/Jurassic boundary has also been reported from changes in nitrogen isotope ratios and fossil biomarker studies from Tethyan and Panthalassic sections (Fujisaki et al., 2020; Jaraula et al., 2013; Kasprak et al., 2015; Richoz et al., 2012). The reducing redox conditions remained prevalent in global oceans through the middle-late Hettangian with first signs of shifts towards oxic environments occurring in the early Sinemurian (Richoz et al., 2012; Ritterbush et al., 2015; Thibodeau et al., 2016).

The fluctuating local redox conditions across the Triassic/Jurassic boundary and their close correspondence with skeletal abundance indicate a connection between water-column anoxia and the reduction in benthic faunal abundance across the extinction boundary. The fluctuating local redox conditions well corresponded to changes in skeletal abundance, indicating water column anoxia as a candidate controlling the benthic faunal abundance through the restriction of aerobic habitat (Figure 10). However, an overarching control, such as climate, which drove increased anoxia in the Jurassic, could also have shaped variation in skeletal abundance. For instance, interaction between temperature and oxygen availability explains the biogeography of many living species through their influences on the ratio of oxygen supply to metabolic demand (Deutsch et al., 2015). In this latter case, redox conditions may not have been directly or entirely responsible for the changes in skeletal abundance but may have remained correlated with skeletal changes due to shared controls (Figure 10).

Geological evidence from the Triassic/Jurassic boundary interval supports the scenario involving shared controls on abundance and redox conditions, for the study sites in the Lombardy Basin and at Mt. Cefalo. Peritidal facies at Mt. Cefalo and shallow-marine facies including oolites in the Lombardy Basin suggest that much of the deposition in the studied sections occurred above fair-weather wave base and that the local water column would have been oxygenated by wind mixing even if the I/Ca proxy recorded the mixing of more poorly oxygenated waters from deeper in the basin due to the slower kinetics of iodide oxidation. Emplacement of the Central Atlantic Magmatic Province (CAMP) at the Triassic/Jurassic boundary is a well-supported candidate for the shared control on skeletal abundance and redox conditions. Carbon dioxide emissions from CAMP led to an increase in atmospheric $CO_2$ (Bachan et al., 2012). Resultant warming (McElwain et al., 1999; Ruhl & Kürschner, 2011) could have driven deoxygenation as evident from observations in modern oceans (Levin, 2018). This warming would have increased the basal metabolic demands of marine organisms and the elevated carbon dioxide concentrations and reduced pH of marine waters would have added to physiological stresses (Deutsch et al., 2015; Gazeau et al., 2013; Pörtner et al., 2004; Figure 10). The combined effects of multiple stressors, especially warming and deoxygenation (Reddin et al., 2020), can potentially account for the lower abundance of skeletal (and non-skeletal) animals in the aftermath of the mass extinction event.

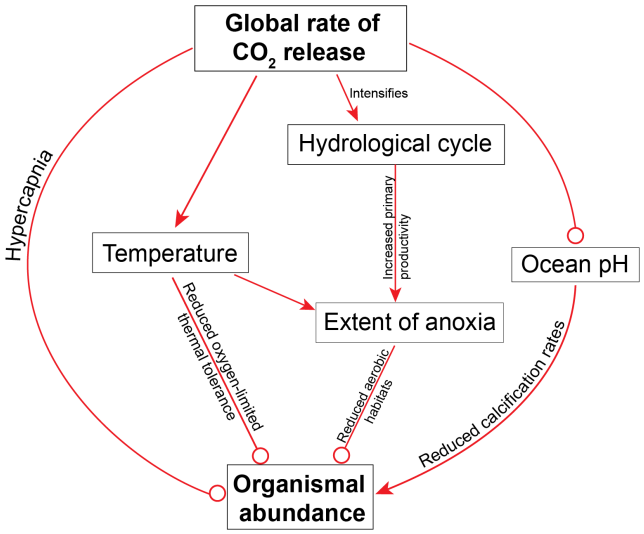


FIGURE 10 A systems analysis model showing the ocean biogeochemical changes associated with CAMP volcanism and its relationship with the Triassic/Jurassic biotic crisis. The parameters connected by arrows indicate a positive coupling between them and a negative coupling between those connected by open circles. For example, physiological effects due to increase in $pCO_2$ will lead to a decrease in skeletal abundance indicating an inverse relationship. Thus, this feedback is represented by an open circle.

Irrespective of the control, the geochemical proxy evidence indicates multiple episodes of carbon dioxide release during the early Hettangian created deleterious environmental conditions by sustaining high temperatures (Huynh & Poulsen, 2005; McElwain et al., 1999) and creating unstable oceanic redox conditions in shallow-marine environments in Early Jurassic. The prolonged hyperthermal and anoxic conditions could have reduced the carrying capacity of Early Jurassic marine ecosystems and delayed recovery until early Sinemurian time.

## 6 | CONCLUSIONS

In this study, we measured skeletal abundance and I/Ca ratios in marine limestones in four Tethyan sections to reconstruct changes in faunal abundance and redox conditions across the Triassic/Jurassic boundary. We find evidence of a significant reduction in skeletal abundance across the end-Triassic extinction event that is reproducible among sections and cannot be explained by changes in depositional environment. I/Ca ratios indicate that the drop in skeletal abundance across the Triassic/Jurassic boundary was accompanied by an expansion of reducing conditions in shallow-marine environments in the regions of deposition. The eventual increase in skeletal abundance in the late Hettangian-Sinemurian is also associated with an increase in I/Ca. This correlation between skeletal abundance and I/Ca ratio indicates that the prevalence of dysoxic to anoxic environments during the early Hettangian was an important factor contributing to the decline in skeletal abundance. We hypothesize that physiological constraints posed by high oceanic temperatures and changing ocean pH resulting from carbon dioxide release during CAMP volcanism acted in tandem with reduced oxygen availability to limit the abundance of skeletal benthic organisms in Hettangian ecosystems.

Changes in abundance of benthic organisms, which are critical to understanding energy flow in ecosystems, have remained among the most difficult to assess across mass extinctions. Studies like this one provide a novel perspective for understanding the ecological severity of mass extinctions, complementary to taxonomic diversity, counts of ecological modes of life, and food-web reconstructions. They also provide a different perspective in directly assessing effects of ongoing, human-induced mass rarity currently underway in modern oceans (Hull, 2015).

## ACKNOWLEDGEMENTS

This study was supported through a graduate research assistantship from Stanford University (to P.S.), NSF EAR 2121445 and NSF OCE 1736542 (to Z.L.), and NSF EAR 2121392 (to J.L.P.). P.S. would like to thank the members of the Payne Paleobiology Lab for thoughtful discussions and feedback. The authors would like to thank the anonymous reviewers whose comments greatly impoved the manuscript.

## CONFLICTS OF INTEREST

The authors have no conflicts of interest to declare.

## DATA AVAILABILITY STATEMENT

The data that support the findings of this study are available from the corresponding author upon reasonable request.

## ORCID

*Pulkit Singh* https://orcid.org/0000-0001-8588-5650
*Zunli Lu* https://orcid.org/0000-0003-4250-3178

## REFERENCES

Aberhan, M., & Kiessling, W. (2015). Persistent ecological shifts in marine molluscan assemblages across the end-Cretaceous mass extinction. *Proceedings of the National Academy of Sciences*, *112*, 7207–7212. https://doi.org/10.1073/pnas.1422248112

Al-Suwaidi, A. H., Steuber, T., & Suarez, M. B. (2016). The Triassic–Jurassic boundary event from an equatorial carbonate platform (Ghalilah Formation, United Arab Emirates). *Journal of the Geological Society*, *173*, 949–953. https://doi.org/10.1144/jgs2015-102

Atkinson, J. W., & Wignall, P. B. (2019). How quick was marine recovery after the end-Triassic mass extinction and what role did anoxia play? *Palaeogeography, Palaeoclimatology, Palaeoecology*, *528*, 99–119. https://doi.org/10.1016/j.palaeo.2019.05.011

Atkinson, J. W., Wignall, P. B., Morton, J. D., & Aze, T. (2019). Body size changes in bivalves of the family Limidae in the aftermath of the end-Triassic mass extinction: The Brobdingnag effect. *Palaeontology*, *62*, 561–582.

Bachan, A., & Payne, J. L. (2016). Modelling the impact of pulsed CAMP volcanism on $pCO_2$ and $\delta^{13}C$ across the Triassic–Jurassic transition. *Geological Magazine*, *153*, 252–270. https://doi.org/10.1017/S0016756815000126

Bachan, A., van de Schootbrugge, B., Fiebig, J., McRoberts, C. A., Ciarapica, G., & Payne, J. L. (2012). Carbon cycle dynamics following the end-Triassic mass extinction: Constraints from paired

$\delta^{13}C_{carb}$ and $\delta^{13}C_{org}$ records. *Geochemistry, Geophysics, Geosystems*, *13*, 1–24. https://doi.org/10.1029/2012GC004150

Bambach, R. K. (2006). Phanerozoic biodiversity mass extinctions. *Annual Review of Earth and Planetary Sciences*, *34*, 127–155.

Bambach, R. K., Knoll, A. H., & Sepkoski, J. J. (2002). Anatomical and ecological constraints on Phanerozoic animal diversity in the marine realm. *Proceedings of the National Academy of Sciences*, *99*, 6854–6859.

Barattolo, F., & Romano, R. (2005). Shallow carbonate platform bioevents during the Upper Triassic-Lower Jurassic: An evolutive interpretation. *Bollettino della Societa Geologica Italiana*, *124*, 123–142.

Barnosky, A. D., Hadly, E. A., Bascompte, J., Berlow, E. L., Brown, J. H., Fortelius, M., Getz, W. M., Harte, J., Hastings, A., Marquet, P. A., & Martinez, N. D. (2012). Approaching a state shift in earth's biosphere. *Nature*, *486*, 52–58.

Barras, C. G., & Twitchett, R. J. (2007). Response of the marine infauna to Triassic–Jurassic environmental change: Ichnological data from southern England. *Palaeogeography, Palaeoclimatology, Palaeoecology*, *244*, 223–241. https://doi.org/10.1016/j.palaeo.2006.06.040

Berra, F. (2012). Sea-level fall, carbonate production, rainy days: How do they relate? Insight from Triassic carbonate platforms (Western Tethys, Southern Alps, Italy). *Geology*, *40*, 271–274. https://doi.org/10.1130/G32803.1

Berra, F., Jadoul, F., & Anelli, A. (2010). Environmental control on the end of the Dolomia Principale/Hauptdolomit depositional system in the central Alps: Coupling sea-level and climate changes. *Palaeogeography, Palaeoclimatology, Palaeoecology*, *290*, 138–150. https://doi.org/10.1016/j.palaeo.2009.06.037

Bertotti, G., Siletto, G. B., & Spalla, M. I. (1993). Deformation and metamorphism associated with crustal rifting: The Permian to Liassic evolution of the Lake Lugano-Lake Como area (Southern Alps). *Tectonophysics*, *226*, 271–284. https://doi.org/10.1016/0040-1951(93)90122-Z

Blackburn, T. J., Olsen, P. E., Bowring, S. A., McLean, N. M., Kent, D. V., Puffer, J., McHone, G., Rasbury, E. T., & Et-Touhami, M. (2013). Zircon U-Pb geochronology links the end-Triassic extinction with the Central Atlantic Magmatic Province. *Science*, *340*, 941–945.

Blois, J. L., Zarnetske, P. L., Fitzpatrick, M. C., & Finnegan, S. (2013). Climate change and the past, present, and future of biotic interactions. *Science*, *341*, 499–504.

Bond, D. P. G., & Grasby, S. E. (2017). On the causes of mass extinctions. *Palaeogeography, Palaeoclimatology, Palaeoecology*, *478*, 3–29. https://doi.org/10.1016/j.palaeo.2016.11.005

Bowman, C. N., Lindskog, A., Kozik, N. P., Richbourg, C. G., Owens, J. D., & Young, S. A. (2020). Integrated sedimentary, biotic, and paleoredox dynamics from multiple localities in southern Laurentia during the late Silurian (Ludfordian) extinction event. *Palaeogeography, Palaeoclimatology, Palaeoecology*, *553*. https://doi.org/10.1016/j.palaeo.2020.109799

Brand, U., & Veizer, J. (1980). Chemical diagenesis of a multicomponent carbonate system; 1, Trace elements. *Journal of Sedimentary Research*, *50*, 1219–1236. https://doi.org/10.1306/212F7BB7-2B24-11D7-8648000102C1865D

Brandano, M., Corda, L., Tomassetti, L., & Tagliavento, M. (2016). Frequency analysis across the drowning of a Lower Jurassic carbonate platform: The Calcare Massiccio Formation (Apennines, Italy). *Marine and Petroleum Geology*, *78*, 606–620. https://doi.org/10.1016/j.marpetgeo.2016.09.013

Brenchley, P. J., Marshall, J. D., & Underwood, C. J. (2001). Do all mass extinctions represent an ecological crisis? Evidence from the Late Ordovician. *Geological Journal*, *36*, 329–340.

Brosse, M., Bucher, H., Baud, A., Frisk, Å. M., Goudemand, N., Hagdorn, H., Nützel, A., Ware, D., & Hautmann, M. (2019). New data from Oman indicate benthic high biomass productivity coupled with low taxonomic diversity in the aftermath of the Permian–Triassic Boundary mass extinction. *Lethaia*, *52*, 165–187.

Bucur, I. I. (1999). Stratigraphic significance of some skeletal algae (Dasycladales, Caulerpales) of the Phanerozoic. In A. Farinacci (Ed.), *Depositional episodes and bioevents* (pp. 53–104). Palaeopelagos Special Publication.

Chance, R., Baker, A. R., Carpenter, L., & Jickells, T. D. (2014). The distribution of iodide at the sea surface. *Environmental Science: Processes & Impacts*, *16*, 1841–1859. https://doi.org/10.1039/C4EM00139G

Christie, M., Holland, S. M., & Bush, A. M. (2013). Contrasting the ecological and taxonomic consequences of extinction. *Paleobiology*, *39*, 538–559.

Ciarapica, G., & Passeri, L. (2005). Late Triassic and Early Jurassic sedimentary evolution of the Northern Apennines: An overview. *Bollettino della Societa Geologica Italiana*, *124*, 189–201.

Cirilli, S., Buratti, N., Gugliotti, L., & Frixa, A. (2015). Palynostratigraphy and palynofacies of the Upper Triassic Streppenosa Formation (SE Sicily, Italy) and inference on the main controlling factors in the organic rich shale deposition. *Review of Palaeobotany and Palynology*, *218*, 67–79. https://doi.org/10.1016/j.revpalbo.2014.10.009

Corsetti, F. A., et al. (2015). Investigating the paleoecological consequences of supercontinent breakup: Sponges clean up in the early Jurassic. *The Sedimentary Record*, *13*, 4–10. https://doi.org/10.2110/sedred.2015.2.4

Coskun Tunaboylu, B., Altiner, D., Isintek, I., & Demirci, D. (2014). Foraminiferal biostratigraphy and sequence stratigraphy of peritidal carbonates at the Triassic–Jurassic boundary (Karaburun Peninsula, Western Turkey). *Journal of Asian Earth Sciences*, *90*, 61–76. https://doi.org/10.1016/j.jseaes.2014.04.015

Cribb, A. T., & Bottjer, D. J. (2020). Complex marine bioturbation ecosystem engineering behaviors persisted in the wake of the end-Permian mass extinction. *Scientific Reports*, *10*, 1–8.

Delecat, S., & Reitner, J. (2005). Sponge communities from the Lower Liassic of Adnet (Northern Calcareous Alps, Austria). *Facies*, *51*, 385–404. https://doi.org/10.1007/s10347-005-0045-x

Deutsch, C., Ferrel, A., Seibel, B., Pörtner, H.-O., & Huey, R. B. (2015). Climate change tightens a metabolic constraint on marine habitats. *Science*, *348*, 1132–1135. https://doi.org/10.1126/science.aaa1605

Di Stefano, P., Favara, R., Luzio, D., Renda, P., Cacciatore, M. S., Calò, M., Napoli, G., Parisi, L., Todaro, S., & Zarcone, G. (2015). A regional-scale discontinuity in western Sicily revealed by a multidisciplinary approach: A new piece for understanding the geodynamic puzzle of the southern Mediterranean. *Tectonics*, *34*, 2067–2085. https://doi.org/10.1002/2014TC003759

Diaz, R. J., & Rosenberg, R. (2008). Spreading dead zones and consequences for marine ecosystems. *Science*, *321*, 926–929.

Dineen, A. A., Roopnarine, P. D., & Fraiser, M. L. (2019). Ecological continuity and transformation after the Permo-Triassic mass extinction in northeastern Panthalassa. *Biology Letters*, *15*(3), p.20180902. https://doi.org/10.1098/rsbl.2018.0902

Droser, M. L., Bottjer, D. J., Sheehan, P. M., & McGhee, G. R., Jr. (2000). Decoupling of taxonomic and ecologic severity of Phanerozoic marine mass extinctions. *Geology*, *28*, 675–678.

Droser, M. L., Jensen, S., & Gehling, J. G. (2002). Trace fossils and substrates of the terminal Proterozoic-Cambrian transition: Implications for the record of early bilaterians and sediment mixing. *Proceedings of the National Academy of Sciences*, *99*, 12572–12576. https://doi.org/10.1073/pnas.202322499

Dunhill, A. M., Foster, W. J., Azaele, S., Sciberras, J., & Twitchett, R. J. (2018). Modelling determinants of extinction across two Mesozoic hyperthermal events. *Proceedings of the Royal Society B: Biological Sciences*, *285*(1889), p.20180404. https://doi.org/10.1098/rspb.2018.0404

Emerson, S., Cranston, R. E., & Liss, P. S. (1979). Redox species in a reducing fjord: Equilibrium and kinetic considerations. *Deep Sea Research Part A. Oceanographic Research Papers*, *26*, 859–878. https://doi.org/10.1016/0198-0149(79)90101-8

Finnegan, S., Rasmussen, C. M., & Harper, D. A. T. (2016). Biogeographic and bathymetric determinants of brachiopod extinction and

survival during the Late Ordovician mass extinction. *Proceedings of the Royal Society B: Biological Sciences*, *283*, 20160007.

Flügel, E. (2010). Quantitative microfacies analysis. In *Microfacies of carbonate rocks: Analysis, interpretation and application* (pp. 243–266). Springer Berlin Heidelberg. https://doi.org/10.1007/978-3-642-03796-2_6

Fox, C. P., Cui, X., Whiteside, J. H., Olsen, P. E., Summons, R. E., & Grice, K. (2020). Molecular and isotopic evidence reveals the end-Triassic carbon isotope excursion is not from massive exogenous light carbon. *Proceedings of the National Academy of Sciences of the United States of America*, *117*, 30171–30178. https://doi.org/10.1073/pnas.1917661117

Fujisaki, W., Fukami, Y., Matsui, Y., Sato, T., Sawaki, Y., & Suzuki, K. (2020). Redox conditions and nitrogen cycling during the Triassic–Jurassic transition: A new perspective from the mid-Panthalassa. *Earth-Science Reviews*, *204*, 103173. https://doi.org/10.1016/j.earscirev.2020.103173

Gaetani, M. (1970). Faune hettangiane della parte orientale della provincia di Bergamo. *Rivista Italiana di Paleontologia e Stratigrafia*, *76*, 355–442.

Galli, M. T., Jadoul, F., Bernasconi, S. M., Cirilli, S., & Weissert, H. (2007). Stratigraphy and palaeoenvironmental analysis of the Triassic–Jurassic transition in the western Southern Alps (Northern Italy). *Palaeogeography, Palaeoclimatology, Palaeoecology*, *244*, 52–70. https://doi.org/10.1016/j.palaeo.2006.06.023

Galli, M. T., Jadoul, F., Bernasconi, S. M., & Weissert, H. (2005). Anomalies in global carbon cycling and extinction at the Triassic/Jurassic boundary: Evidence from a marine C-isotope record. *Palaeogeography, Palaeoclimatology, Palaeoecology*, *216*, 203–214. https://doi.org/10.1016/j.palaeo.2004.11.009

Gazeau, F., Parker, L. M., Comeau, S., Gattuso, J.-P., O'Connor, W. A., Martin, S., Pörtner, H.-O., & Ross, P. M. (2013). Impacts of ocean acidification on marine shelled molluscs. *Marine Biology*, *160*, 2207–2245. https://doi.org/10.1007/s00227-013-2219-3

Ge, Y., Shi, M., Steuber, T., Al-Suwaidi, A. H., & Suarez, M. B. (2018). Environmental change during the Triassic–Jurassic boundary interval of an equatorial carbonate platform: Sedimentology and chemostratigraphy of the Ghalilah Formation, United Arab Emirates. *Palaeogeography, Palaeoclimatology, Palaeoecology*, *502*, 86–103. https://doi.org/10.1016/j.palaeo.2018.04.026

Greene, S. E., Bottjer, D. J., Hagdorn, H., & Zonneveld, J.-P. (2011). The Mesozoic return of Paleozoic faunal constituents: A decoupling of taxonomic and ecological dominance during the recovery from the end-Permian mass extinction. *Palaeogeography, Palaeoclimatology, Palaeoecology*, *308*, 224–232.

Haas, J., Kovács, S., Krystyn, L., & Lein, R. (1995). Significance of Late Permian-Triassic facies zones in terrane reconstructions in the Alpine-North Pannonian domain. *Tectonophysics*, *242*, 19–40. https://doi.org/10.1016/0040-1951(94)00157-5

Häntzschel, W., & Reineck, H. E. (1968). Fazies-Untersuchungen im Hettangium von Helmstedt (Niedersachsen). *Mitteilungen aus dem Geologischen Staatsinstitut in Hamburg*, *37*, 5–39.

Hardisty, D. S., Lu, Z., Bekker, A., Diamond, C. W., Gill, B. C., Jiang, G., Kah, L. C., Knoll, A. H., Loyd, S. J., Osburn, M. R., & Planavsky, N. J. (2017). Perspectives on Proterozoic surface ocean redox from iodine contents in ancient and recent carbonate. *Earth and Planetary Science Letters*, *463*, 159–170. https://doi.org/10.1016/j.epsl.2017.01.032

Harnik, P. G., Simpson, C., & Payne, J. L. (2012). Long-term differences in extinction risk among the seven forms of rarity. *Proceedings of the Royal Society B: Biological Sciences*, *279*, 4969–4976.

Hautmann, M. (2004). Effect of end-Triassic CO 2 maximum on carbonate sedimentation and marine mass extinction. *Facies*, *50*, 257–261.

He, T., Dal Corso, J., Newton, R. J., Wignall, P. B., Mills, B. J., Todaro, S., Di Stefano, P., Turner, E. C., Jamieson, R. A., Randazzo, V., & Rigo, M. (2020). An enormous sulfur isotope excursion indicates marine anoxia during the end-Triassic mass extinction. *Science Advances*, *6*, eabb6704. https://doi.org/10.1126/sciadv.abb6704

He, T., Newton, R. J., Wignall, P. B., Reid, S., Dal Corso, J., Takahashi, S., Wu, H., Todaro, S., Di Stefano, P., Randazzo, V., & Rigo, M. (2022). Shallow ocean oxygen decline during the end-Triassic mass extinction. *Global and Planetary Change*, *210*, 103770. https://doi.org/10.1016/j.gloplacha.2022.103770

He, T., Wignall, P. B., Newton, R. J., Atkinson, J. W., Keeling, J. F. J., Xiong, Y., & Poulton, S. W. (2022). Extensive marine anoxia in the European epicontinental sea during the end-Triassic mass extinction. *Global and Planetary Change*, *210*, 103771. https://doi.org/10.1016/j.gloplacha.2022.103771

Hull, P. (2015). Life in the aftermath of mass extinctions. *Current Biology*, *25*, R941–R952. https://doi.org/10.1016/j.cub.2015.08.053

Hull, P. M. (2017). Emergence of modern marine ecosystems. *Current Biology*, *27*, R466–R469. https://doi.org/10.1016/j.cub.2017.04.041

Hull, P. M., & Darroch, S. A. F. (2013). Mass extinctions and the structure and function of ecosystems. *The Paleontological Society Papers*, *19*, 115–156.

Hull, P. M., Norris, R. D., Bralower, T. J., & Schueth, J. D. (2011). A role for chance in marine recovery from the end-Cretaceous extinction. *Nature Geoscience*, *4*, 856–860.

Huynh, T. T., & Poulsen, C. J. (2005). Rising atmospheric $CO_2$ as a possible trigger for the end-Triassic mass extinction. *Palaeogeography, Palaeoclimatology, Palaeoecology*, *217*, 223–242. https://doi.org/10.1016/j.palaeo.2004.12.004

Iannace, A., & Zamparelli, V. (2002). Upper Triassic platform margin biofacies and the paleogeography of Southern Apennines. *Palaeogeography, Palaeoclimatology, Palaeoecology*, *179*, 1–18. https://doi.org/10.1016/S0031-0182(01)00362-5

Jacobsen, N. D., Twitchett, R. J., & Krystyn, L. (2011). Palaeoecological methods for assessing marine ecosystem recovery following the Late Permian mass extinction event. *Palaeogeography, Palaeoclimatology, Palaeoecology*, *308*, 200–212. https://doi.org/10.1016/j.palaeo.2010.04.024

Jadoul, F., Berra, F., & Frisia, S. (1992). Stratigraphic and paleogeographic evolution of a carbonate platform in an extensional tectonic regime: The example of the Dolomia Principale in Lombardy (Italy). *Rivista Italiana di Paleontologia e Stratigrafia*, *98*, 29–44. https://doi.org/10.13130/2039-4942/8939

Jadoul, F., & Galli, M. T. (2008). The Hettangian shallow water carbonates after the Triassic/Jurassic biocalcification crisis: The Albenza Formation in the Western Southern Alps. *Rivista Italiana di Paleontologia e Stratigrafia*, *114*, 453–470. https://doi.org/10.13130/2039-4942/5911

Jadoul, F., Galli, M. T., Berra, F., Cirilli, S., Ronchi, P., & Paganoni, A. M. (2004). *The Late Triassic-Early Jurassic of the Lombardy Basin: Stratigraphy, palaeogeography and palaeontology. Field guide book escursion P86*.

Jadoul, F., Galli, M. T., Calabrese, L., & Gnaccolini, M. (2005). Stratigraphy of Rhaetian to Lower Sinemurian carbonate platforms in western Lombardy (Southern Alps, Italy): Paleogeographic implications. *Rivista Italiana di Paleontologia e Stratigrafia*, *111*, 285–303.

Jaraula, C. M. B., Grice, K., Twitchett, R. J., Böttcher, M. E., LeMetayer, P., Dastidar, A. G., & Opazo, L. F. (2013). Elevated $pCO_2$ leading to Late Triassic extinction, persistent photic zone euxinia, and rising sea levels. *Geology*, *41*, 955–958. https://doi.org/10.1130/G34183.1

Jost, A. B., Bachan, A., van de Schootbrugge, B., Brown, S. T., DePaolo, D. J., & Payne, J. L. (2017). Additive effects of acidification and mineralogy on calcium isotopes in Triassic/Jurassic boundary limestones. *Geochemistry, Geophysics, Geosystems*, *18*, 113–124. https://doi.org/10.1002/2016GC006724

Jost, A. B., Bachan, A., van de Schootbrugge, B., Lau, K. V., Weaver, K. L., Maher, K., & Payne, J. L. (2017). Uranium isotope evidence for an expansion of marine anoxia during the end-Triassic extinction.

*Geochemistry, Geophysics, Geosystems*, *18*, 3093–3108. https://doi.org/10.1002/2017GC006941

Kasprak, A. H., Sepúlveda, J., Price-Waldman, R., Williford, K. H., Schoepfer, S. D., Haggart, J. W., Ward, P. D., Summons, R. E., & Whiteside, J. H. (2015). Episodic photic zone euxinia in the northeastern Panthalassic Ocean during the end-Triassic extinction. *Geology*, *43*, 307–310. https://doi.org/10.1130/G36371.1

Kiessling, W., & Aberhan, M. (2007). Environmental determinants of marine benthic biodiversity dynamics through Triassic–Jurassic time. *Paleobiology*, *33*, 414–434.

Kiessling, W., Aberhan, M., Brenneis, B., & Wagner, P. J. (2007). Extinction trajectories of benthic organisms across the Triassic–Jurassic boundary. *Palaeogeography, Palaeoclimatology, Palaeoecology*, *244*, 201–222.

Knaust, D. (2010). The end-Permian mass extinction and its aftermath on an equatorial carbonate platform: Insights from ichnology. *Terra Nova*, *22*, 195–202.

Knoll, A. H., Bambach, R. K., Canfield, D. E., & Grotzinger, J. P. (1996). Comparative Earth history and Late Permian mass extinction. *Science*, *273*, 452–457.

Knoll, A. H., Bambach, R. K., Payne, J. L., Pruss, S., & Fischer, W. W. (2007). Paleophysiology and end-Permian mass extinction. *Earth and Planetary Science Letters*, *256*, 295–313. https://doi.org/10.1016/j.epsl.2007.02.018

Knoll, A. H., Summons, R. E., Waldbauer, J. R., & Zumberge, J. E. (2007). CHAPTER 8 – The geological succession of primary producers in the oceans. In P. G. Falkowski & A. H. Knoll (Eds.), *Evolution of primary producers in the sea* (pp. 133–163). Academic Press. https://doi.org/10.1016/B978-012370518-1/50009-6

Lakew, T. (1990). Microfacies and cyclic sedimentation of the Upper Triassic (Rhaetian) Calcare di zu (Southern Alps). *Facies*, *22*, 187–231. https://doi.org/10.1007/BF02536952

Lakew, T. (1994). Diagenesis of a Rhaetian patch reef (Lombardian basin, southern Alps). *Rivista Italiana di Paleontologia e Stratigrafia*, *100*, 9–32.

Larina, E., Bottjer, D. J., Corsetti, F. A., Zonneveld, J. P., Celestian, A. J., & Bailey, J. V. (2019). Uppermost Triassic phosphorites from Williston Lake, Canada: link to fluctuating euxinic-anoxic conditions in northeastern Panthalassa before the end-Triassic mass extinction. *Scientific Reports*, *9*, 1–9. https://doi.org/10.1038/s41598-019-55162-2

Levin, L. A. (2018). Manifestation, drivers, and emergence of open ocean deoxygenation. *Annual Review of Marine Science*, *10*, 229–260. https://doi.org/10.1146/annurev-marine-121916-063359

Lu, W., Ridgwell, A., Thomas, E., Hardisty, D. S., Luo, G., Algeo, T. J., Saltzman, M. R., Gill, B. C., Shen, Y., Ling, H. F., & Edwards, C. T. (2018). Late inception of a resiliently oxygenated upper ocean. *Science*, *361*, 174–177. https://doi.org/10.1126/science.aar5372

Lu, Z., Hoogakker, B. A. A., Hillenbrand, C.-D., Zhou, X., Thomas, E., Gutchess, K. M., Lu, W., Jones, L., & Rickaby, R. E. M. (2016). Oxygen depletion recorded in upper waters of the glacial Southern Ocean. *Nature Communications*, *7*, 11146. https://doi.org/10.1038/ncomms11146

Lu, Z., Jenkyns, H. C., & Rickaby, R. E. M. (2010). Iodine to calcium ratios in marine carbonate as a paleo-redox proxy during oceanic anoxic events. *Geology*, *38*, 1107–1110. https://doi.org/10.1130/G31145.1

Lu, Z., Lu, W., Rickaby, R. E. M., & Thomas, E. (2020). *Earth history of oxygen and the iprOxy*. Cambridge University Press, Elements in Geochemical Tracers in Earth System Science. https://doi.org/10.1017/9781108688604

Mancinelli, A., Chiocchini, M., Chiocchini, R. A., & Romano, A. (2005). Biostratigraphy of Upper Triassic-Lower Jurassic carbonate platform sediments of the central-southern Apennines (Italy). *Rivista Italiana di Paleontologia e Stratigrafia*, *111*, 271–283. https://doi.org/10.13130/2039-4942/6314

Mariotti, G., Pruss, S. B., Perron, J. T., & Bosak, T. (2014). Microbial shaping of sedimentary wrinkle structures. *Nature Geoscience*, *7*, 736–740. https://doi.org/10.1038/ngeo2229

Mata, S. A., & Bottjer, D. J. (2009). The paleoenvironmental distribution of Phanerozoic wrinkle structures. *Earth-Science Reviews*, *96*, 181–195. https://doi.org/10.1016/j.earscirev.2009.06.001

McCauley, D. J., Pinsky, M. L., Palumbi, S. R., Estes, J. A., Joyce, F. H., & Warner, R. R. (2015). Marine defaunation: Animal loss in the global ocean. *Science*, *347*(6219), p.1255641. https://doi.org/10.1126/science.1255641

McElwain, J. C., Beerling, D. J., & Woodward, F. I. (1999). Fossil plants and global warming at the Triassic–Jurassic boundary. *Science*, *285*, 1386–1390. https://doi.org/10.1126/science.285.5432.1386

McGhee, G. R., Clapham, M. E., Sheehan, P. M., Bottjer, D. J., & Droser, M. L. (2013). A new ecological-severity ranking of major Phanerozoic biodiversity crises. *Palaeogeography, Palaeoclimatology, Palaeoecology*, *370*, 260–270. https://doi.org/10.1016/j.palaeo.2012.12.019

McGhee, G. R., Jr., Sheehan, P. M., Bottjer, D. J., & Droser, M. L. (2004). Ecological ranking of Phanerozoic biodiversity crises: Ecological and taxonomic severities are decoupled. *Palaeogeography, Palaeoclimatology, Palaeoecology*, *211*, 289–297.

McRoberts, C. A. (1994). The Triassic–Jurassic ecostratigraphic transition in the Lombardian Alps, Italy. *Palaeogeography, Palaeoclimatology, Palaeoecology*, *110*, 145–166. https://doi.org/10.1016/0031-0182(94)90114-7

McRoberts, C. A., Furrer, H., & Jones, D. S. (1997). Palaeoenvironmental interpretation of a Triassic–Jurassic boundary section from Western Austria based on palaeoecological and geochemical data. *Palaeogeography, Palaeoclimatology, Palaeoecology*, *136*, 79–95. https://doi.org/10.1016/S0031-0182(97)00074-6

Muttoni, G., Kent, D. V., Jadoul, F., Olsen, P. E., Rigo, M., Galli, M. T., & Nicora, A. (2010). Rhaetian magneto-biostratigraphy from the Southern Alps (Italy): Constraints on Triassic chronology. *Palaeogeography, Palaeoclimatology, Palaeoecology*, *285*, 1–16. https://doi.org/10.1016/j.palaeo.2009.10.014

Pálfy, J., Demény, A., Haas, J., Carter, E. S., Görög, Á., Halász, D., Oravecz-Scheffer, A., Hetényi, M., Márton, E., Orchard, M. J., & Ozsvárt, P. (2007). Triassic–Jurassic boundary events inferred from integrated stratigraphy of the Csővár section, Hungary. *Palaeogeography, Palaeoclimatology, Palaeoecology*, *244*, 11–33. https://doi.org/10.1016/j.palaeo.2006.06.021

Pálfy, J., Kovács, Z., Demény, A., & Vallner, Z. (2021). End-riassic crisis and unreefing led to the demise of the Dachstein carbonate platform: A revised model and evidence from the Transdanubian Range, Hungary. *Global and Planetary Change*, *199*, 103428. https://doi.org/10.1016/j.gloplacha.2021.103428

Payne, J. L. (2005). Evolutionary dynamics of gastropod size across the end-Permian extinction and through the Triassic recovery interval. *Paleobiology*, *31*, 269–290. https://doi.org/10.1666/0094-8373(2005)031[0269:EDOGSA]2.0.CO;2

Payne, J. L., Lehrmann, D. J., Wei, J., & Knoll, A. H. (2006). The pattern and timing of biotic recovery from the end-Permian extinction on the Great Bank of Guizhou, Guizhou Province, China. *Palaios*, *21*, 63–85. https://doi.org/10.2110/palo.2005.p05-12p

Payne, J. L., & Van de Schootbrugge, B. (2007). CHAPTER 9 – Life in Triassic oceans: Links between planktonic and benthic recovery and radiation. In P. G. Falkowski & A. H. Knoll (Eds.), *Evolution of primary producers in the sea* (pp. 165–189). Academic Press. https://doi.org/10.1016/B978-012370518-1/50010-2

Penn, J. L., Deutsch, C., Payne, J. L., & Sperling, E. A. (2018). Temperature-dependent hypoxia explains biogeography and severity of end-Permian marine mass extinction. *Science*, *362*, eaat1327. https://doi.org/10.1126/science.aat1327

Peterffy, O., Calner, M., & Vajda, V. (2016). Early Jurassic microbial mats—A potential response to reduced biotic activity in the aftermath of the end-Triassic mass extinction event. *Palaeogeography, Palaeoclimatology, Palaeoecology*, *464*, 76–85. https://doi.org/10.1016/j.palaeo.2015.12.024

Pörtner, H. O., Langenbuch, M., & Reipschläger, A. (2004). Biological impact of elevated ocean $CO_2$ concentrations: Lessons from animal physiology and earth history. *Journal of Oceanography*, *60*, 705–718.

Pruss, S., Fraiser, M., & Bottjer, D. J. (2004). Proliferation of Early Triassic wrinkle structures: Implications for environmental stress following the end-Permian mass extinction. *Geology*, *32*, 461–464. https://doi.org/10.1130/G20354.1

Raup, D. M., & Sepkoski, J. J. (1982). Mass extinctions in the marine fossil record. *Science*, *215*, 1501–1503.

Reddin, C. J., Nätscher, P. S., Kocsis, Á. T., Pörtner, H. O., & Kiessling, W. (2020). Marine clade sensitivities to climate change conform across timescales. *Nature Climate Change*, *10*, 249–253. https://doi.org/10.1038/s41558-020-0690-7

Richoz, S., Van De Schootbrugge, B., Pross, J., Püttmann, W., Quan, T. M., Lindström, S., Heunisch, C., Fiebig, J., Maquil, R., Schouten, S., & Hauzenberger, C. A. (2012). Hydrogen sulphide poisoning of shallow seas following the end-Triassic extinction. *Nature Geoscience*, *5*, 662–667. https://doi.org/10.1038/ngeo1539

Ritterbush, K. A., Bottjer, D. J., Corsetti, F. A., & Rosas, S. (2014). New evidence on the role of siliceous sponges in ecology and sedimentary facies development in eastern Panthalassa following the Triassic–Jurassic mass extinction. *Palaios*, *29*, 652–668. https://doi.org/10.2110/palo.2013.121

Ritterbush, K. A., Ibarra, Y., & Tackett, L. S. (2016). Post-extinction biofacies of the first carbonate ramp of the early Jurassic (Sinemurian) in NE Panthalassa (New York Canyon, Nevada, USA). *Palaios*, *31*, 141–160. https://doi.org/10.2110/palo.2015.021

Ritterbush, K. A., Rosas, S., Corsetti, F. A., Bottjer, D. J., & West, A. J. (2015). Andean sponges reveal long-term benthic ecosystem shifts following the end-Triassic mass extinction. *Palaeogeography, Palaeoclimatology, Palaeoecology*, *420*, 193–209. https://doi.org/10.1016/j.palaeo.2014.12.002

Romano, R., Masett, D., Carras, N., Barattolo, F., & Roghi, G. (2008). The triassic/jurassic boundary in a peritidal carbonate platform of the pelagonian domain: The mount messapion section (Chalkida, Greece). *Rivista Italiana di Paleontologia e Stratigrafia*, *114*, 431–452. https://doi.org/10.13130/2039-4942/5910

Roopnarine, P. D., & Angielczyk, K. D. (2015). Community stability and selective extinction during the Permian-Triassic mass extinction. *Science*, *350*, 90–93.

Ruhl, M., & Kürschner, W. M. (2011). Multiple phases of carbon cycle disturbance from large igneous province formation at the Triassic–Jurassic transition. *Geology*, *39*, 431–434. https://doi.org/10.1130/G31680.1

Scheffer, M., Carpenter, S., & de Young, B. (2005). Cascading effects of overfishing marine systems. *Trends in Ecology & Evolution*, *20*, 579–581.

Schettino, A., & Turco, E. (2011). Tectonic history of the western Tethys since the Late Triassic. *GSA Bulletin*, *123*, 89–105. https://doi.org/10.1130/B30064.1

Schubert, J. K., & Bottjer, D. J. (1995). Aftermath of the Permian-Triassic mass extinction event: Paleoecology of Lower Triassic carbonates in the western USA. *Palaeogeography, Palaeoclimatology, Palaeoecology*, *116*, 1–39.

Scotese, C. R. (2016). *Tutorial: PALEOMAP PaleoAtlas for GPlates and the PaleoData Plotter program, PALEOMAP Project*. https://doi.org/10.13140/RG2.2.34367.00166

Sepkoski, J. J., Bambach, R. K., Raup, D. M., & Valentine, J. W. (1981). Phanerozoic marine diversity and the fossil record. *Nature*, *293*, 435–437.

Sibert, E. C., Hull, P. M., & Norris, R. D. (2014). Resilience of Pacific pelagic fish across the Cretaceous/Palaeogene mass extinction. *Nature Geoscience*, *7*, 667–670. https://doi.org/10.1038/ngeo2227

Stampfli, G. M., Borel, G. D., Cavazza, W., Mosar, J., & Ziegler, P. A. (2001). Palaeotectonic and palaeogeographic evolution of the western Tethys and PeriTethyan domain (IGCP Project 369). *Episodes*, *24*, 222–227. https://doi.org/10.18814/epiiugs/2001/v24i4/001

Thibodeau, A. M., Ritterbush, K., Yager, J. A., West, A. J., Ibarra, Y., Bottjer, D. J., Berelson, W. M., Bergquist, B. A., & Corsetti, F. A. (2016). Mercury anomalies and the timing of biotic recovery following the end-Triassic mass extinction. *Nature Communications*, *7*, 11147. https://doi.org/10.1038/ncomms11147

Todaro, S., Di Stefano, P., Zarcone, G., & Randazzo, V. (2017). Facies stacking and extinctions across the Triassic–Jurassic boundary in a peritidal succession from western Sicily. *Facies*, *63*, 1–21. https://doi.org/10.1007/s10347-017-0500-5

Todaro, S., Hollis, C., & Di Stefano, P. (2016). Spongy-like porosity in peritidal carbonates: An interaction of cyclic sea-level oscillations, fresh water supply and sediment texture. *Sedimentary Geology*, *333*, 70–83. https://doi.org/10.1016/j.sedgeo.2015.12.005

Todaro, S., Rigo, M., Randazzo, V., & Di Stefano, P. (2018). The end-Triassic mass extinction: A new correlation between extinction events and $\delta^{13}C$ fluctuations from a Triassic–Jurassic peritidal succession in western Sicily. *Sedimentary Geology*, *368*, 105–113. https://doi.org/10.1016/j.sedgeo.2018.03.008

Truesdale, V. W., Bale, A. J., & Woodward, E. M. S. (2000). The meridional distribution of dissolved iodine in near-surface waters of the Atlantic Ocean. *Progress in Oceanography*, *45*, 387–400. https://doi.org/10.1016/S0079-6611(00)00009-4

Twitchett, R. J., & Barras, C. G. (2004). Trace fossils in the aftermath of mass extinction events. *Geological Society, London, Special Publications*, *228*, 397–418.

Van de Schootbrugge, B., Payne, J. L., Tomasovych, A., Pross, J., Fiebig, J., Benbrahim, M., Föllmi, K. B., & Quan, T. M. (2008). Carbon cycle perturbation and stabilization in the wake of the Triassic–Jurassic boundary mass-extinction event. *Geochemistry, Geophysics, Geosystems*, *9*,Q04028. https://doi.org/10.1029/2007GC001914

Van de Schootbrugge, B., Tremolada, F., Rosenthal, Y., Bailey, T. R., Feist-Burkhardt, S., Brinkhuis, H., Pross, J., Kent, D. V., & Falkowski, P. G. (2007). End-Triassic calcification crisis and blooms of organic-walled "disaster species". *Palaeogeography, Palaeoclimatology, Palaeoecology*, *244*, 126–141. https://doi.org/10.1016/j.palaeo.2006.06.026

Wagner, P. J., Kosnik, M. A., & Lidgard, S. (2006). Abundance distributions imply elevated complexity of post-Paleozoic marine ecosystems. *Science*, *314*, 1289–1292.

Wong, G. T. F., & Brewer, P. G. (1977). The marine chemistry of iodine in anoxic basins. *Geochimica et Cosmochimica Acta*, *41*, 151–159. https://doi.org/10.1016/0016-7037(77)90195-8

Wray, J. J. (1977). Late Paleozoic calcareous red algae. In E. Flügel (Ed.), *Fossil algae* (pp. 167–176). Springer Berlin Heidelberg.

Zhou, X., Jenkyns, H. C., Owens, J. D., Junium, C. K., Zheng, X. Y., Sageman, B. B., Hardisty, D. S., Lyons, T. W., Ridgwell, A., & Lu, Z. (2015). Upper ocean oxygenation dynamics from I/Ca ratios during the Cenomanian-Turonian OAE 2. *Paleoceanography*, *30*, 510–526. https://doi.org/10.1002/2014PA002741

Zhou, X., Thomas, E., Rickaby, R. E. M., Winguth, A. M. E., & Lu, Z. (2014). I/Ca evidence for upper ocean deoxygenation during the PETM. *Paleoceanography*, *29*, 964–975. https://doi.org/10.1002/2014PA002702

## SUPPORTING INFORMATION

Additional supporting information can be found online in the Supporting Information section at the end of this article.

**How to cite this article:** Singh, P., Lu, W., Lu, Z., Jost, A. B., Lau, K., Bachan, A., van de Schootbrugge, B., & Payne, J. L. (2023). Reduction in animal abundance and oxygen availability during and after the end-Triassic mass extinction. *Geobiology*, *21*, 175–192. https://doi.org/10.1111/gbi.12533